

# Star formation in bright-rimmed clouds and cluster associated with W5 E HII region

Neelam Chauhan<sup>1\*</sup>, A. K. Pandey<sup>1</sup>, K. Ogura<sup>2</sup>, J. Jose<sup>1</sup>, D. K. Ojha<sup>3</sup>,  
M. R. Samal<sup>1</sup>, H. Mito<sup>4</sup>

<sup>1</sup>*Aryabhatta Research Institute of observational sciencES (ARIES), Nainital, 263 129, India*

<sup>2</sup>*Kokugakuin University, Higashi, Shibuya-ku, Tokyo 150-8440, Japan*

<sup>3</sup>*Tata Institute of Fundamental Research, Mumbai (Bombay) - 400 005, India*

<sup>4</sup>*Kiso Observatory, School of Science, University of Tokyo, Mitake, Kiso-machi, Kiso-gun, Nagano-ken 397-0101, Japan*

## ABSTRACT

The aim of this paper is to present the results of photometric investigations of the central cluster of the W5 E region as well as a follow-up study of the triggered star formation in and around bright-rimmed clouds (BRCs). We have carried out wide field  $UBVI_c$  and deep  $VI_c$  photometry of the W5 E HII region. A distance of  $\sim 2.1$  kpc and a mean age of  $\sim 1.3$  Myr have been obtained for the central cluster. The young stellar objects (YSOs) associated with the region are identified on the basis of near-infrared and mid-infrared observations. We confirmed our earlier results that the average age of the YSOs lying on/inside the rim are younger than those lying outside the rim. The global distribution of the YSOs shows an aligned distribution from the ionising source to the BRCs. These facts indicate that a series of radiation driven implosion processes proceeded from near the central ionising source towards the periphery of the W5 E HII region. We found that, in general, the age distributions of the Class II and Class III sources are the same. This result is apparently in contradiction with the conclusion by Bertout, Siess & Cabrit (2007) and Chauhan et al. (2009) that classical T Tauri stars evolve to weak-line T Tauri stars. The initial mass function of the central cluster region in the mass range  $0.4 \leq M/M_\odot \leq 30$  can be represented by  $\Gamma = -1.29 \pm 0.03$ . The cumulative mass functions indicate that in the mass range  $0.2 \leq M/M_\odot \leq 0.8$ ,

the cluster region and BRC NW have more low mass YSOs in comparison to BRCs 13 and 14.

**Key words:** stars : formation - stars : pre-main-sequence - ISM : globules  
HII regions - open cluster: initial mass function; star formation.

## 1 INTRODUCTION

Massive stars have a profound effect on the evolution of their natal molecular clouds. Their strong stellar winds and ultraviolet (UV) radiation cause an important feedback of energy and momentum in the surrounding medium. Once massive stars form they begin to ionise the remaining parental molecular cloud. The ionising UV radiation has two competing effects on the parental molecular cloud. One is negative feedback on star formation activity, i.e., the remaining molecular cloud is dispersed and further star formation is halted. The other is positive feedback. The interaction can trigger new episodes of star formation as the HII region expands into the molecular cloud. Two processes have been considered for the triggering of star formation at the edge of the HII region, namely ‘collect and collapse’ and ‘radiation driven implosion (RDI)’. In the collect and collapse process, a compressed layer of high density neutral material is accumulated between the ionisation front (IF) and the shock front (SF). The dynamical instabilities in the compressed layer result in the fragmentation of the layer and formation of second generation stars.

If the IF/ SF encounters pre-existing denser parts, it compresses them to induce star formation. The process is known as RDI. Detailed model calculations of the RDI process have been carried out by several authors (e.g., Bertoldi 1989, Lefloch & Lazareff 1995, Kessel-Deynet & Burkert 2003, Miao et al. 2006). Star formation is predicted to occur in **the** initial short compression phase. This compression phase is followed by a transient phase of re-expansion and then by a quasi-stationary cometary phase. During this last phase, the cloud represents a structure of a dense head and a long tail and moves slowly away from the ionising source by the rocket effect. The signature of the RDI process is the anisotropic density distribution of gas in a relatively small molecular cloud surrounded by a curved ionisation front (bright rim) as well as a small group of YSOs in front of it.

BRCs are small molecular clouds located near the edge of evolved HII regions and show signs of the RDI and are hence considered to be good laboratories to study the physical

processes involved in the RDI process. Sugitani et al. (1995) carried out near infrared (NIR) imaging of 44 BRCs and found that elongated small clusters or aggregates of YSOs, which are aligned toward the direction of the ionizing star, are often associated with them. These aggregates showed a tendency that ‘redder’ (presumably younger) stars tend to be located inside the BRCs, whereas relatively ‘bluer’ (presumably older) stars are found outside the clouds, suggesting an age gradient. Thus, they advocated a hypothesis called ‘*small-scale sequential star formation ( $S^4F$ )*’. If the BRC is originally relatively large, the star formation may propagate along the axis of the BRCs as the ionization/shock front advances further and further into the molecular cloud (Kessel-Deynet & Burkert 2003).

The W5 HII region is an extended HII region with relatively simple morphology and shows indications of triggered star formation. It is a part of the large W3/W4/W5 cloud complex in the Perseus arm and consists of two adjacent circular HII regions, W5 E and W5 W. There are many studies on this region. Karr & Martin (2003) discussed triggered star formation in W5 using multi-wavelength archival data. Based on the timescales of the expansion of the HII region and the age of the YSOs, they obtained the timescale of the interaction between the molecular clouds and the HII region,  $t \sim 0.5 - 1.0$  Myr. Using the *Spitzer* Space Telescope imaging with Infrared Array Camera (IRAC) and Multiband Imaging Photometer for *Spitzer* (MIPS), Koenig et al. (2008) noticed dense clusters of YSOs, centered around the O stars HD 17505, HD 17520, BD +60 586 and HD 18326. The HII region W5 E is primarily ionised by HD 18326. Chauhan et al. (2009) also paid attention to the cluster around this O7 V star. W5 E HII region has two BRCs, namely BRCs 13 and 14 (Sugitani et al. 1991, hereafter SFO 91) at its periphery. Based on the column densities of  $^{13}\text{CO}$  and the spatial distribution of YSO candidates, Niwa et al. (2009) identified a BRC candidate in the north-western part of the W5 E HII region. We refer to this BRC candidate as BRC NW. Hence W5 E is an interesting region to study triggered star formation.

In our earlier papers (Ogura et al. 2007, hereafter Paper I; Chauhan et al. 2009, hereafter Paper II) we have studied the star formation scenario in/ around six BRCs, including BRCs 13 and 14. The analysis was limited to the YSOs detected using the  $\text{H}\alpha$  emission and NIR excess only. A recent study by Koenig et al. (2008) has increased the number of YSOs in W5 E significantly. Hence, these data can be used to further investigate the YSO contents which we partly failed to detect in the  $\text{H}\alpha$  and NIR excess surveys reported in Paper I and Paper II.

In this paper, we have made an attempt to make photometric studies of the stellar content

of the newly identified cluster in W5 E, by incorporating the NIR and mid infrared (MIR) data from IRAC/ MIPS of the *Spitzer* telescope. We have also considered the properties of the YSOs in the cluster as well as the three BRC regions to understand the star formation scenario in the W5 E HII region. The influence of the ionizing source on the surrounding parental molecular cloud has also been discussed.

In Sections 2 and 3, we describe the observations, data reductions and archival data used in the present work. Section 4 describes the analysis of the associated cluster. Sections 5 and 6 illustrate the procedure to estimate the membership, age, mass of the YSOs and total-to-selective extinction,  $R_V$  in the cluster and BRC regions. In Section 7 we discuss the initial mass function (IMF) and cumulative mass functions (CMFs) of the cluster and BRC regions. Section 8 describes the star formation scenario in the cluster and BRC regions. In Section 9 the disk evolution of T Tauri Stars (TTs) has been discussed.

## 2 OBSERVATIONS AND DATA REDUCTIONS

The  $50 \times 50$  arcmin<sup>2</sup> area containing the cluster around the O7 star HD 18326 that is noticed by Koenig et al. (2008) and Chauhan et al. (2009), is reproduced from the DSS2-R image, and shown in Fig. 1. As is evident from the figure, the cluster is embedded in an HII region W5 E. BRCs 13 and 14 are located towards the eastern side, whereas BRC NW detected by Niwa et al. (2009) can be seen towards the north-west direction of the cluster. In the ensuing subsections we describe the observations carried out to study the region in detail.

### 2.1 Optical CCD Observations

The  $UBVI_c$  CCD optical observations of W5 E were carried out using the the  $2048 \times 2048$  pixel<sup>2</sup> CCD camera mounted at the f/3.1 Schmidt focus of the 1.05-m telescope of Kiso Observatory, Japan. The pixel size of  $24 \mu\text{m}$  with an image scale of  $1''.5/\text{pixel}$  covers a field of view of  $\sim 50 \times 50$  arcmin<sup>2</sup> on the sky. The average FWHM of the star images during the observations was  $\sim 3''$ .

The  $UBVI_c$  CCD observations of the central region of W5 E have also been carried out using the  $2048 \times 2048$  pixel<sup>2</sup> CCD camera mounted on the 1.04-m Sampurnanand Telescope (ST) of the Aryabhata Research Institute of Observational Sciences (ARIES), Nainital, India. To improve the signal-to-noise ratio (S/N), the observations were carried out in a binning mode of  $2 \times 2$  pixel<sup>2</sup>. The pixel size is  $24 \mu\text{m}$  with an image scale of  $0''.37/\text{pixel}$  and

**Table 1.** Log of observations

$\alpha_{(2000)}$ (h:m:s)	$\delta_{(2000)}$ (d:m:s)	Filter & Exposure(sec)×no. of frames	Date of observations (yr-mm-dd)
KISO			
02:59:22.60	+60:33:48.7	U:180×9,30×6; B:60×9,10×6; V:60×9,10×6; I:60×9,10×6	2007-10-20
ST			
02:59:22.60	+60:33:48.7	U:240×2,10×1; B:180×2,5×1; V:100×2,4×1; I:60×2,4×1	2009-10-13
02:59:22.60	+60:33:48.7	U:900×1,300×1; B:600×5; V:360×9; I:120×10	2006-12-16
03:00:08.34	+60:39:19.3	V:600×5;I:300×5	2007-10-13
02:58:38.78	+60:39:06.1	V:600×5;I:300×5	2007-10-13
03:00:03.49	+60:27:59.6	V:600×5;I:300×5	2007-10-13
02:58:33.34	+60:28:47.2	V:300×10;I:300×5	2007-11-06
02:57:44.41	+60:38:29.1	V:180×2;I:100×2	2009-10-13
02:57:44.41	+60:38:29.1	V:600×6;I:300×8	2009-10-15
02:59:34.13	+61:05:28.4	V:300×10;I:300×5	2006-12-15
HCT			
02:59:23.83	+60:34:00.0	Gr7/167l:300×1	2009-11-16

the entire chip covers a field of  $\sim 13 \times 13$  arcmin<sup>2</sup> on the sky. The average FWHM of star images was  $\sim 2''.5$ . The observations of the central region of W5 E were standardised on 2009 October 13 by observing standard stars in the SA 92 field (Landolt 1992). Deep imaging of a nearby field region towards the north from the cluster centre ( $\alpha_{2000} = 02^h59^m34^s$ ;  $\delta_{2000} = +61^\circ05'28''$ ), was also carried out in  $V$  and  $I_c$  bands using the ST. The magnitudes of bright stars which were saturated in deep exposure frames have been taken from short exposure frames. A number of bias and twilight frames were also taken during the observing runs. The log of the observations is tabulated in Table 1.

The pre-processing of the data frames was done using the various tasks available under the *IRAF* data reduction software package. The photometric measurements of the stars were performed using the *DAOPHOTII* software package (Stetson 1987). The point spread function was obtained for each frame using several uncontaminated stars.

The instrumental magnitudes of the central region observed on 2009 October 13 with ST were converted into the standard system using least-square linear regression procedures outlined by Stetson (1992). The photometric calibration equations used are as follows:

$$u = U + (7.858 \pm 0.007) + (0.596 \pm 0.024)X + (0.124 \pm 0.008)(U - B),$$

$$b = B + (5.464 \pm 0.006) + (0.336 \pm 0.010)X + (0.134 \pm 0.006)(B - V),$$

$$v = V + (5.088 \pm 0.006) + (0.188 \pm 0.011)X + (0.032 \pm 0.007)(V - I_c),$$

$$i = I_c + (5.320 \pm 0.012) + (0.121 \pm 0.019)X + (0.106 \pm 0.011)(V - I_c)$$

where  $U, B, V$  and  $I_c$  are the standard magnitudes;  $u, b, v$  and  $i$  are the instrumental magnitudes obtained after time and aperture corrections and  $X$  is the airmass. We have ignored

the second-order colour correction terms as they are generally small in comparison with other errors present in the photometric data reduction. The standard deviations of the standardisation residuals,  $\Delta$ , between the standard and transformed magnitudes and colours of the standard stars, are found to be  $\Delta V = 0.008$ ,  $\Delta(B - V) = 0.017$ ,  $\Delta(V - I_c) = 0.020$  and  $\Delta(U - B) = 0.011$ . The photometric accuracies depend on the brightness of the stars, and the typical *DAOPHOT* errors in  $B$ ,  $V$  and  $I_c$  bands at  $V \sim 18$  are smaller than 0.01 mag. Near the limiting magnitude of  $V \sim 21$ , the *DAOPHOT* errors increase to 0.06 and 0.04 mag in the  $V$  and  $I_c$  bands, respectively. The Kiso data were standardised using the secondary standards obtained from the central region observations as mentioned above.

To study the luminosity function (LF)/ mass function (MF) of the cluster region we have used  $VI_c$  data taken with ST. It is necessary to take into account the incompleteness in the observed data that may occur for various reasons (e.g., crowding of the stars). A quantitative evaluation of the completeness of the photometric data with respect to the brightness and the position on a given frame is necessary to convert the observed LF to a true LF. We used the ADDSTAR routine of *DAOPHOTII* to determine the completeness factor (CF). The procedure has been outlined in detail in our earlier works (see e.g., Pandey et al. 2001). We randomly added artificial stars to both  $V$  and  $I_c$  images in such a way that they have similar geometrical locations but differ in  $I_c$  brightness according to the mean  $(V - I_c)$  colour ( $=1.5$  mag) of the data sample. The luminosity distribution of artificial stars is chosen in such a way that more stars are inserted towards the fainter magnitude bins. The frames are reduced using the same procedure used for the original frame. The ratio of the number of stars recovered to that added in each magnitude interval gives the CF as a function of magnitude. The minimum value of the CF of the pair (i.e.,  $V$  and  $I_c$  band observations) for the two sub-regions, given in Table 2, is used to correct the data for incompleteness. The incompleteness of the data increases with increasing magnitude as expected. However, it does not depend on the area significantly.

The photometric results for the BRC 13 and BRC 14 regions have been taken from our earlier work (Paper II). They are based on observations with Himalayan Faint Object Spectrograph Camera (HFOSC) on the 2.0-m Himalayan Chandra Telescope (HCT). The boundaries of the earlier observations are shown with dashed lines in Fig. 1.

**Table 2.** Completeness factor of photometric data in the cluster and field regions.

V range (mag)	cluster region $r \leq 3'$	$3' < r \leq 6'$	field region
13.5 - 14.0	1.00	1.00	1.00
14.0 - 14.5	1.00	1.00	1.00
14.5 - 15.0	0.99	0.99	1.00
15.0 - 15.5	0.98	0.98	0.99
15.5 - 16.0	0.98	0.98	0.98
16.0 - 16.5	0.96	0.97	0.98
16.5 - 17.0	0.97	0.96	0.98
17.0 - 17.5	0.97	0.96	0.98
17.5 - 18.0	0.95	0.95	0.96
18.0 - 18.5	0.93	0.94	0.95
18.5 - 19.0	0.91	0.92	0.94
19.0 - 19.5	0.88	0.90	0.91
19.5 - 20.0	0.85	0.84	0.89
20.0 - 20.5	0.81	0.82	0.84
20.5 - 21.0	0.72	0.71	0.77
21.0 - 21.5	0.51	0.54	0.57

## 2.2 Grism Slit spectroscopy

We obtained a low resolution optical spectrum of the exciting star of W5 E, HD 18326, on 2009 November 16 using HFOSC on HCT, with a slit width of 2 arcsec and Grism 7 ( $\lambda = 3800 - 6840 \text{ \AA}$ , dispersion =  $1.45 \text{ \AA/pixel}$ ). A one dimensional spectrum was extracted from the bias subtracted and flat-field corrected image in the standard manner using IRAF. The wavelength calibration of the spectrum was done using a FeAr lamp source. The standard star G191-B2B is used for the standardisation and flux calibration.

## 3 ARCHIVAL DATA

### 3.1 Near-infrared data from 2MASS

NIR  $JHK_s$  data for point sources within a radius of  $25'$  around the central cluster have been obtained from the Two Micron All Sky Survey (2MASS) Point Source Catalog (PSC) (Cutri et al. 2003). Sources having uncertainty less than 0.1 mag ( $S/N \geq 10$ ) in all the three bands were selected to ensure high quality data. The  $JHK_s$  data were transformed from the 2MASS system to the CIT system using the relations given at the 2MASS website<sup>1</sup>.

### 3.2 Mid-infrared data from *Spitzer*

The near- and mid-infrared data ( $3.6$  to  $24 \text{ }\mu\text{m}$ ) from the *Spitzer* Space telescope have provided the capability to detect and measure the infrared excesses due to circumstellar

<sup>1</sup> <http://www.astro.caltech.edu/~jmc/2mass/v3/transformations/>

disk emission of the YSOs. In order to study the evolutionary stages of the YSOs detected using the *Spitzer*, we used IRAC (3.6  $\mu\text{m}$ , 4.5  $\mu\text{m}$ , 5.8  $\mu\text{m}$  and 8.0  $\mu\text{m}$ ) and MIPS (24  $\mu\text{m}$ ) photometry taken from Koenig et al. (2008).

### 3.3 H $\alpha$ emission stars from slitless spectroscopy

The H $\alpha$  emission stars for the cluster region and BRC regions have been taken from Nakano et al. (2008) and Ogura et al. (2002), respectively.

## 4 ANALYSIS OF THE ASSOCIATED CLUSTER

### 4.1 Radial stellar surface density profile

The radial extent is one of the important parameters to study the dynamical properties of clusters. To estimate this we assumed a spherically symmetric distribution of stars in the cluster. The star count technique is one of the useful tools to determine the distribution of cluster stars with respect to the surrounding stellar background.

In order to determine the cluster centre, we derived the highest peak of stellar density by fitting a Gaussian profile to the star counts in strips along both the X and Y axes around the eye estimated cluster centre. The cluster centre from the optical data has turned out to be at  $\alpha_{2000} = 02^{\text{h}}59^{\text{m}}22^{\text{s}}.0 \pm 1^{\text{s}}.0$ ;  $\delta_{2000} = +60^{\circ}34'37'' \pm 12''$ . We repeated the same procedure using the 2MASS data to estimate the cluster centre and obtained it to be  $\sim 12''$  away from the optical co-ordinates. However, this difference is within the uncertainty. Henceforth, we adopt the optical centre.

We estimated the radial density profile (RDP) to study the radial structure of the cluster. We divided the cluster into a number of concentric circles and the projected stellar density in each concentric annulus was obtained by dividing the number of stars by the respective annulus area. Stars brighter than  $V = 19.5$  mag and  $K = 14.7$  mag were considered for estimating the RDPs from the optical and 2MASS data, respectively. The densities thus obtained are plotted as a function of radius in Fig. 2. The error bars are derived assuming that the number of stars in each annulus follows the Poisson statistics.

The extent of the cluster  $r_{cl}$  is defined as the radius where the cluster stellar density merges with the field stellar density. The horizontal dashed line in the plot shows the field star density, which is obtained from a region  $\sim 25'$  away towards the north from the cluster centre ( $\alpha_{2000} = 02^{\text{h}}59^{\text{m}}34^{\text{s}}$ ;  $\delta_{2000} = +61^{\circ}05'28''$ ). Based on the radial density profile, we find

that the  $r_{cl}$  is about  $6'$  for stars brighter than  $V = 19.5$  mag. Almost the same value for the cluster extent is obtained for the 2MASS data. We adopted a radius of  $6'$  for this cluster to obtain the cluster parameters such as reddening, distance, IMF etc.

To parameterise the RDP of the cluster, we fitted the observed RDP with the empirical model of King (1962) which is given by

$$\rho(r) \propto \frac{\rho_0}{1 + \left(\frac{r}{r_c}\right)^2},$$

where  $r_c$  is the core radius at which the surface density  $\rho(r)$  becomes half of the central density,  $\rho_0$ . The best fit to the radial density obtained by a  $\chi^2$  minimization technique, is shown in Fig. 2. The core radius thus estimated is  $1'.01 \pm 0'.12$ .

## 4.2 Interstellar reddening

We know that the extinction or reddening  $E(B - V)$  of a star in a cluster arises due to two distinct sources:

- (i) the general interstellar medium (ISM) in the foreground of the cluster  $[E(B - V)_f]$ , and
- (ii) the localized ISM associated with the cluster  $[E(B - V)_c = E(B - V) - E(B - V)_f]$ ,

The former component is characterised by the ratio of the total-to-selective extinction  $R_V$   $[= A_V / E(B - V)] = 3.1$  (Wegner 1993; He et al. 1995; Winkler 1997), whereas, for the intra-cluster regions of young clusters embedded in a dust and gas cloud, the value of  $R_V$  may vary significantly (Chini & Wargau 1990; Tapia et al. 1991; Pandey et al. 2000). The value of  $R_V$  affects the distance determination significantly, and consequently the age determination of stars. Several studies have already pointed out **an** anomalous reddening law with high  $R_V$  values in the vicinity of star forming regions (see e.g., Neckel & Chini 1981, Chini & Krüegel 1983, Chini & Wargau 1990, Pandey et al. 2000, Samal et al. 2007). Since the W5 E cluster and the BRCs are associated with the HII region, it will be interesting to examine the reddening law in these objects. The ratio of total-to-selective extinction  $R_V$  is found to be normal in the cluster region (cf. Section 6 for details).

Since spectroscopic observations are not available, the interstellar reddening  $E(B - V)$  towards the cluster region is estimated using the  $(U - B)/(B - V)$  colour-colour (CC) diagram. The CC diagram of the cluster region is presented in Fig. 3. Since the cluster is very young, a variable reddening within the cluster region is expected. In Fig. 3, the continuous

lines represent the intrinsic zero age main sequence (ZAMS) by Girardi et al. (2002) which are shifted by  $E(B - V) = 0.62$  and  $0.80$  mag respectively, along the normal reddening vector (i.e.,  $E(U - B)/E(B - V) = 0.72$ ) to match the distributions of probable cluster members. Fig. 3 thus yields a variable reddening with  $E(B - V)_{min} = 0.62$  mag to  $E(B - V)_{max} = 0.80$  mag in the cluster region. The stars lying within these two reddened ZAMSs may be probable members of the cluster. Reddening of individual stars with spectral classes earlier than A0 have been computed using the reddening free index,  $Q$  (Johnson & Morgan 1953). Assuming a normal reddening law, we calculated  $Q = (U - B) - 0.72 \times (B - V)$ . The value of  $Q$  for stars earlier than A0 will be  $< 0$ . For main sequence (MS) stars, the intrinsic  $(B - V)_0$  colour and colour excess can be obtained by the relations;  $(B - V)_0 = 0.332 \times Q$  and  $E(B - V) = (B - V) - (B - V)_0$ , respectively. Fig. 3 also indicates a large amount of contamination due to field stars. The probable late type foreground stars with spectral types later than A0 may follow the ZAMS reddened by  $E(B - V) = 0.50$  mag. A careful inspection of Fig. 3 indicates the presence of further reddened background populations. The reddening  $E(B - V)$  for the background population is found out to be in the range of  $\sim 0.95$  -  $1.25$  mag. This population may belong to the blue plume (BP) of the Norma-Cygnus arm (cf. Pandey et al. 2006). The estimated  $E(B - V)$  values for the background population are comparable to the  $E(B - V)$  value of the BP population around  $l \sim 130^\circ$  (cf. Pandey et al. 2006).

### 4.3 Spectral classification of the ionising star in W5 E HII region

We obtained a slit spectrum of the brightest source to study its nature. In Fig. 4, we present the flux calibrated, normalised spectrum of HD 18326, which is the ionising source of the HII region, in the wavelength range  $3990 - 5000 \text{ \AA}$ . The important lines have been identified and labeled. HD 18326 is identified as an O7V and O7V(n) type star by Conti & Leep (1974) and Walborn (1973), respectively. The ratio of HeI  $\lambda 4471$ / HeII  $\lambda 4542$  is a primary indicator of the spectral class of early type stars. The ratio we found for this star is  $\sim 1$ , which indicates that it is an  $O7 \pm 0.5$  star. With the present resolution of the spectrum, luminosity assessment is quite difficult. However, due to the presence of strong absorption in HeII  $\lambda 4686$ , we assign the luminosity class V.

#### 4.4 Distance and optical colour magnitude diagrams

The spectral class of the ionising source yields an intrinsic distance modulus of 11.2 which corresponds to a distance of 1.74 kpc. Here, it is worthwhile noting that the  $M_V$  for an O7V star in the literature varies significantly; e.g.,  $M_V = -5.2$  (Schmidt-Kaler 1982) to  $-4.9$  (Martins & Plez 2006). This star is also reported as a variable star and a suspected spectroscopic binary (Kazarovets et al. 1998; Turner et al. 2008). Hence, the distance estimation based only on the O-type star alone may not be reliable. We also estimated the individual distance modulus of other probable MS stars. The intrinsic colours for each star were estimated using the Q-method as discussed in Sec. 4.2. We estimated corresponding  $M_V$  values for each star using the ZAMS by Girardi et al. (2002). The average value of the intrinsic distance modulus, obtained using 24 probable MS members, comes out to be  $11.65 \pm 0.57$ , corresponding to a distance of  $2.1 \pm 0.3$  kpc. This distance estimate is in agreement with those obtained by Becker & Fenkart (1971; 2.2 kpc), Georgelin & Georgelin (1976; 2.0 kpc) and Hillwig et al. (2006; 1.9 kpc).

We used the optical colour magnitude diagrams (CMDs) to derive the fundamental parameters of the cluster, such as age, distance etc. The  $V/(B - V)$  and  $V/(V - I)$  CMDs for stars lying within  $6'$  radius are shown in Figs. 5a and 5b. Fig. 5c shows the  $V/(V - I)$  CMD for a nearby field region (see Sec. 4.1). A 4 Myr isochrone for  $Z = 0.019$  by Girardi et al. (2002) and the pre-main-sequence (PMS) isochrones for 1 Myr and 5 Myr by Siess et al. (2000) have also been plotted for  $(m - M_V) = 13.5$  mag and  $E(B - V) = 0.62$  mag assuming  $E(V - I) = 1.25 \times E(B - V)$  and  $R_V = 3.1$ . A comparison of the CMDs of the cluster region with the field region reveals an unambiguous population of PMS sources along with a significant contamination due to field star population.

### 5 IDENTIFICATION OF PRE-MAIN-SEQUENCE OBJECTS ASSOCIATED WITH THE CLUSTER AND BRCS

Since the W5 E region is located at a low galactic latitude, the region is significantly contaminated by foreground/background stars as discussed above. In order to understand star formation in the region, we selected probable PMS members associated with the region using the following criteria.

Some PMS stars, specifically classical T Tauri stars (CTTSs), show emission lines in their spectra, among which usually  $H\alpha$  is the strongest. Therefore,  $H\alpha$  emission stars can be

considered as good candidates for PMS stars associated with the region. In the present study, we use  $H\alpha$  emission stars found by Ogura et al. (2002) and Nakano et al. (2008) in the W5 E HII region. Since many PMS stars also show NIR/MIR excesses caused by circumstellar disks, NIR/MIR photometric surveys are also powerful tools to detect low-mass PMS stars. We have also used the YSOs identified by Koenig et al. (2008) in the W5 E HII region using *Spitzer* IRAC and MIPS photometry.

Fig. 6a shows the NIR  $(J - H)/(H - K)$  colour-colour (NIR-CC) diagram of all the sources detected in the 2MASS catalogue along with the YSOs identified by Koenig et al. (2008) in the cluster region, whereas Fig. 6b shows the NIR-CC diagram for the sources in the nearby reference field. In Figs. 6a and 6b, the thin and long-dashed curves represent the unreddened MS and giant branches (Bessell & Brett 1988), respectively. The dotted line indicates the locus of intrinsic CTTSs (Meyer et al. 1997). The curves are also in the CIT system. The parallel dashed lines are the reddening vectors drawn from the tip (spectral type M4) of the giant branch (“upper reddening line”), from the base (spectral type A0) of the MS branch (“middle reddening line”) and from the tip of the intrinsic CTTS line (“lower reddening line”). The extinction ratios  $A_J/A_V = 0.265$ ,  $A_H/A_V = 0.155$  and  $A_K/A_V = 0.090$  have been adopted from Cohen et al. (1981). We classified sources into three regions in the NIR-CC diagrams (cf. Ojha et al. 2004a). ‘F’ sources are located between the upper and middle reddening lines and are considered to be either field stars (MS stars, giants) or Class III sources and Class II sources with small NIR excesses. ‘T’ sources are located between the middle and lower reddening lines. These sources are considered to be mostly CTTSs (Class II objects). There may be an overlap in NIR colours of Herbig Ae/Be stars and CTTSs in the ‘T’ region (Hillenbrand et al. 1992). ‘P’ sources are those located in the region redward of the ‘T’ region and are most likely Class I objects (protostar-like objects; Ojha et al. 2004b). So, objects falling in the ‘T’ and ‘P’ regions of NIR-CC diagrams are considered to be NIR excess stars and hence are probable members of the cluster. These sources are included in the analysis of the present study in addition to  $H\alpha$  emission stars. It is worthwhile, however, to note that Robitaille et al. (2006) have recently shown that there is a significant overlap between protostars and CTTSs in the NIR-CC space.

The  $V/(V - I)$  CMD for the YSOs taken from the catalogue by Koenig et al. (2008) for the cluster region ( $r_{cl} = 6'$ ) is shown in Fig. 7. Here the well-known age-with-mass trend that higher mass stars look older than lower mass stars (Hillenbrand et al. 2008) is evident.

In addition a few sources, having  $V \gtrsim 15$ , classified as Class III objects are located near the MS. They are also located on the MS in the NIR-CC diagram and hence could be field stars. This indicates that part of Class III objects by Koenig et al. (2008) are not YSOs, but rather stars found in the W5 Spitzer photometric sample that appear to have photospheric colours in the 3 to 24  $\mu\text{m}$  bands and thus appear as Class III SEDs. Thus, the listed Class III objects by Koenig et al. (2008) may be heavily contaminated by foreground and background field populations. A comparison of the NIR-CC diagram of the cluster region and nearby field region indicates that the YSOs identified by Koenig et al. (2008) and having  $(J - H) > 0.7$  mag and  $(H - K) > 0.3$  mag can be safely considered as YSOs associated with the region.

The NIR-CC diagrams for the identified YSOs (with  $\text{H}\alpha$  emission and IR excess) in the BRC NW, BRC 13 and BRC 14 are shown in Figs. 8a, 8b and 8c, respectively. The NIR-CC diagrams were used to estimate  $A_V$  for each of these YSOs by tracing them back to the intrinsic CTTS locus of Meyer et al. (1997) along the reddening vector (for details see Paper I & Paper II). The  $A_V$  for the stars lying in the ‘F’ region is estimated by tracing them back to the extension of the intrinsic CTTS locus. The mean reddening for each **BRC** region is calculated. The mean  $A_V$  values for BRC NW, BRC 13 and BRC 14 are found to be 2.26 mag, 2.33 mag and 3.05 mag, respectively. Fig. 9 shows the  $V/(V - I)$  CMDs of the YSOs selected using the NIR-CC diagram in the cluster region as well as in the three BRC regions. Again, the CMDs indicate that practically all of them are PMS stars but, at the same time reveal a significant scatter in their age. The age of each YSO was estimated by referring to the isochrones. The mass of the YSOs was estimated using the  $V/(V - I_c)$  colour-magnitude diagram as discussed in Pandey et al. (2008) and Chauhan et al. (2009). The resultant age and mass are given in Table 3, which is available in an electronic form. Here, we would like to point out that the estimation of the age of the PMS stars by comparing the observations with the theoretical isochrones is prone to two kinds of errors; random errors in observations and systematic errors due to the variation between the predictions of different theoretical evolutionary tracks (see e.g., Hillenbrand 2005, Hillenbrand et al. 2008). The effect of random errors in determination of age and mass was estimated by propagating the random errors to their observed estimation by assuming normal error distribution and using Monte-Carlo simulations. The use of different PMS evolutionary models give different ages and hence an age spread in a cluster (e.g., Sung et al. 2000). In the present study, we have used the models by Siess et al. (2000) only for all the BRCs and the cluster region, therefore our age and mass estimations are not affected by the systematic errors. However, the use of different

**Table 3.** The  $B$ ,  $V$  and  $I_c$  photometric data along with their position, mass and age for the YSOs in the cluster and BRC regions

S. No.	$\alpha_{2000}$ $h : m : s$	$\delta_{2000}$ $d : m : s$	$B \pm eB$ $mag$	$V \pm eV$ $mag$	$I \pm eI$ $mag$	$Age \pm \sigma$ $Myr$	$mass \pm \sigma$ $M_{\odot}$
<b>cluster region</b>							
1	02 : 58 : 39.03	60 : 37 : 25.8	—	$19.67 \pm 0.02$	$16.78 \pm 0.02$	$0.7 \pm 0.01$	$0.4 \pm 0.00$
2	02 : 58 : 39.24	60 : 37 : 02.7	$20.07 \pm 0.02$	$18.21 \pm 0.01$	$15.60 \pm 0.01$	$0.2 \pm 0.02$	$0.5 \pm 0.00$
3	02 : 58 : 39.32	60 : 35 : 00.6	—	$20.78 \pm 0.03$	$18.05 \pm 0.02$	$2.4 \pm 0.05$	$0.4 \pm 0.01$
—	—	—	—	—	—	—	—
—	—	—	—	—	—	—	—

sets of PMS evolutionary tracks will introduce a systematic shift in age determination. The presence of binaries may be another source of errors in the age determination. Binarity will brighten the star, consequently the CMD will yield a lower age estimate. In the case of equal mass binaries we expect an error of  $\sim 50 - 60\%$  in the age estimation of the PMS stars. However, it is difficult to estimate the influence of binarity on the mean age estimation as the fraction of binaries is not known.

## 6 REDDENING LAW IN THE CLUSTER AND BRC REGIONS

To study the nature of the extinction law in the region, we used two colour diagrams (TCDs) as described by Pandey et al. (2003). The TCDs of the form of  $(V - \lambda)$  vs.  $(B - V)$ , where  $\lambda$  is one of the broad-band filters ( $R, I, J, H, K, L$ ), provide an effective method of separating the influence of the normal extinction produced by the diffuse interstellar medium from that of the abnormal extinction arising within regions having a peculiar distribution of dust sizes (cf. Chini & Wargau 1990, Pandey et al. 2000).

The TCDs for the Class III YSOs associated with the cluster and BRC regions are shown in Figs. 10a - 10d. In order to avoid IR excess stars, we have used all the *Spitzer* Class III sources having  $V < 17$  mag. The slopes of the distributions are given in the figure. The ratio of total-to-selective extinction ' $R_V$ ' in the regions is estimated using the procedure described in Pandey et al. (2003). The  $R_V$  values in the cluster and BRC regions, i.e., BRC NW, BRC 13 and BRC 14 are estimated to be  $R_{cluster} = 3.14 \pm 0.12$ ,  $R_{BRCNW} = 3.46 \pm 0.20$ ,  $R_{BRC13} = 3.41 \pm 0.03$  and  $R_{BRC14} = 2.75 \pm 0.12$ , respectively. The value of  $R_{cluster}$  indicates a normal reddening law in the cluster region. The higher values of  $R_{BRCNW}$  and  $R_{BRC13}$  indicate a larger grain size in the BRC NW and BRC 13 regions, whereas the smaller value of  $R_{BRC14}$  suggests a smaller grain size in the case of BRC 14. This indicates that the evolution of dust grains in the W5 E region has not taken place in a homogeneous way.

## 7 MASS FUNCTIONS OF THE CLUSTER AND BRC REGIONS

### 7.1 Initial mass function of the cluster

The IMF is the distribution of the mass of stars at the time of a star formation event. Young clusters are preferred sites for IMF studies as their mass functions (MFs) can be considered as IMFs, since they are too young to lose significant number of members either due to dynamical evolution or stellar evolution. The IMF is defined as the number of stars per unit logarithmic mass interval, and is generally represented by a power law having a slope,

$$\Gamma = d \log N(\log m) / d \log m,$$

where  $N(\log m)$  is the number of stars per unit logarithmic mass interval. For the mass range  $0.4 < M/M_{\odot} \leq 10$ , the classical value derived by Salpeter (1955) is  $\Gamma = -1.35$ .

To study the MF and LF, it is necessary to eliminate the field star contamination from the cluster region. In the absence of proper motion data, one can use statistical criteria to estimate the number of probable member stars in the cluster region. To remove the contamination due to field stars from the MS and PMS sample, we statistically subtracted the contribution of field stars from the observed CMD of the cluster region using the following procedure. For any star in the  $V/(V-I)$  CMD of the control field (Fig. 5c), the nearest star in the cluster's  $V/(V-I)$  CMD (Fig. 5b) within  $V \pm 0.125$  and  $(V-I) \pm 0.065$  was removed. The statistically cleaned CMD is shown in Fig. 11, which clearly shows a sequence of PMS stars. The PMS isochrones by Siess et al. (2000) for age of 0.1 and 5 Myr (dashed lines) and the 4 Myr isochrone by Girardi et al. (2002) (continuous line) are shown in Fig. 11. The evolutionary tracks by Siess et al. (2000) for different masses are also shown which are used to estimate the mass of PMS stars. Here we would like to **note** that the points shown by filled circles in Fig. 11 may not represent the actual members of the clusters. However, the filled circles should represent the statistics of PMS stars that can be used to study the MF of the cluster region. We used the statistics of the sources having age  $0.1 \leq \text{age} \leq 5$  Myr in the statistically cleaned CMD (Fig. 11) to study the IMF of the cluster region. It is also important to make corrections in the data sample for incompleteness which may be due to various reasons, e.g., crowding of the stars. We determined the CF as described in Sec. 2.1. Since the MS age of the most massive star in the cluster is  $< 4$  Myr, the stars having  $V < 14.7$  mag ( $M > 3M_{\odot}$ ) have been considered on the MS. In order to obtain the MF for MS stars, the LF is converted to MF using the theoretical model of Girardi et al. (2002). The

**Table 4.** Cumulative mass function of the YSOs in the cluster and BRC regions

Region	CMF in the mass range	
	$0.8 \leq M/M_{\odot} \leq 1.2$	$0.2 \leq M/M_{\odot} \leq 0.8$
Cluster	$-2.54 \pm 0.40$	$-1.97 \pm 0.28$
BRC NW	$-5.06 \pm 3.18$	$-2.63 \pm 0.21$
BRC 13	$-6.45 \pm 2.01$	$-0.98 \pm 0.14$
BRC 14	$-4.69 \pm 0.75$	$-1.08 \pm 0.14$

MF of the PMS stars was obtained by counting the number of stars in different mass bins (for details see Pandey et al. 2008, Jose et al. 2008). Fig. 12 shows the MF of the cluster in the mass range  $0.4 \leq M/M_{\odot} \leq 30$ . A single slope for the MF in the mass range  $0.4 \leq M/M_{\odot} \leq 30$  can be fitted with  $\Gamma = -1.29 \pm 0.03$ , which is comparable to the Salpeter value (-1.35).

## 7.2 Cumulative mass function of identified YSOs in the cluster and BRC regions

The MF is an important tool to compare the star formation process/scenario in different regions. Morgan et al. (2008), based on SCUBA observations, have estimated the mass of 47 dense cores within the heads of 44 BRCs. They concluded that the slope of the MF of these cores is significantly shallower than that of the Salpeter MF. They also concluded that it depends on the morphological type of BRCs (for the morphological description of BRCs we refer to SFO 91): ‘A’ type BRCs appear to follow the mass spectrum of the clumps in the Orion B molecular cloud, whereas the BRCs of the ‘B’ and ‘C’ types have a significantly shallower MF.

In Paper II, we have studied the CMFs of YSOs selected on the basis of NIR excess and H $\alpha$  emission and found that the ‘A’ type BRCs seem to follow a MF similar to that found in young open clusters, whereas ‘B/C’ type BRCs have a significantly steeper CMF, indicating that BRCs of the latter type tend to form relatively low mass YSOs in the mass range  $0.2 \leq M/M_{\odot} \leq 0.8$ . The CMF of the YSOs associated with the ‘A’ type BRCs in the mass range  $0.2 \leq M/M_{\odot} \leq 0.8$  is found to be comparable with the CMF of the average Galactic IMF (cf. Paper II).

As mentioned above, in Paper II, the YSOs were selected on the basis of NIR excess and H $\alpha$  emission. To make the sample statistically significant we combined the data of different types of BRCs lying in different star forming regions. Since star formation and evolution of TTSS in and around BRCs may depend on the prevailing conditions in the region, it will be

worthwhile to re-investigate the CMF of the YSOs (identified in the present work) in BRC NW, BRCs 13 and 14 as well as those associated with the cluster region. Fig. 13 compares the CMFs of the YSOs in the BRC regions and the cluster region presuming that the biases (if any) in all the four samples are the same. It is interesting to note that the CMFs of the three BRCs show a break in the slope at  $\sim 0.8 M_{\odot}$ . The slopes of the CMFs are given in Table 4, which indicate that in the case of three BRCs, the slopes in the mass range  $0.8 \leq M/M_{\odot} \leq 1.2$  are almost the same. However, in the mass range  $0.2 \leq M/M_{\odot} \leq 0.8$ , the slopes in the BRCs 13 and 14 are found to be similar, whereas CMF in BRC NW and the central cluster are biased towards lower mass in comparison to the BRCs 13 and 14. The average Galactic IMF in the mass range  $0.2 \leq M/M_{\odot} \leq 0.6$ , i.e.,  $\Gamma = -0.3$  (Kroupa 2001, 2002) corresponds to the slope of the CMF of  $-1.1 \pm 0.1$ . This fact also indicates that the cluster region and BRC NW have relatively more low mass YSOs in the mass range  $0.2 \leq M/M_{\odot} \leq 0.8$ .

## 8 STAR FORMATION SCENARIO IN W5 E

The W5 E region is an excellent example of triggered star formation. The presence of central O7 MS star HD 18326 and several bright-rim like structures makes this region an interesting object to study triggered star formation. This region contains two of the BRCs catalogued in SFO 91. The millimeter line study by Niwa et al. (2009) has revealed the presence of a  $^{13}\text{CO}$  cloud and  $\text{C}^{18}\text{O}$  cores on the eastern and northern sides of the region but there is no evidence for clouds on the southern side. They also found high density clumps in the BRC NW region. Karr & Martin (2003) concluded that the exciting O stars and YSOs along the edges of the whole W5 E HII region belong to two different generations. Based on the expansion velocity of the HII region and the evolutionary stages of the IRAS YSOs, they concluded that the timescale is consistent with the triggering by the RDI process.

In our earlier work (Paper I and Paper II) we have studied the star formation scenario in and around BRCs using the YSOs selected on the basis of  $\text{H}\alpha$  emission and NIR excess and found evidence for triggered star formation around BRCs 13 and 14. Nakano et al. (2008) detected several  $\text{H}\alpha$  emission stars in the W5 E region. They found that the young stars near the exciting stars are systematically older ( $\sim 4$  Myr) than those near the edge of the HII region ( $\sim 1$  Myr) and concluded that the formation of stars proceeded sequentially from the centre of the HII region to the eastern bright rims. Based on the observations of IR excess

stars, we proposed in Paper II the occurrence of a series of RDI events in this particular region.

Koenig et al. (2008) have carried out an extensive *Spitzer* survey of the whole IC 1848 region. On the basis of the large-scale distribution of YSOs selected using *Spitzer* data, they found that the ratio of Class II to Class I sources within the HII region cavity is  $\sim 7$  times higher compared to the regions associated with the molecular cloud. They attributed this difference to an age difference between the two locations and concluded that there exist at least two distinct generations of stars in the region. They stated that the triggering is a plausible mechanism to explain the multiple events of star formation and suggested that the W5 HII region merits further investigation.

Earlier works studying the star formation scenario in the region were often qualitative (e.g., Karr & Martin 2003, Koenig et al. 2008). Some were quantitative studies, but they were based on a smaller sample of stars (e.g., Nakano et al. 2008, Papers I and II). Since in the present work we have a larger database, it will be worthwhile studying the global scenario of star formation in the region. In the following subsections we shall study the star formation scenario in the cluster as well as around the BRCs.

## 8.1 Cluster region

The CMD of the identified YSOs (Fig. 9a) and the statistically cleaned CMD (Fig. 11) reveal a non-coeval star formation in the cluster region. The age distribution is shown in Fig. 14. The mean age of the YSOs is estimated to be  $1.26 \pm 0.69$  Myr. This is smaller than the average age of the YSOs obtained by Nakano et al. (2008, age  $\sim 4$  Myr). Nakano et al. (2008) have used only  $H\alpha$  emission stars while the present sample is larger, including NIR and MIR excess stars in addition. To estimate the age of the  $H\alpha$  emission stars, Nakano et al. (2008) used PMS isochrones by Palla & Stahler (1999), whereas we have used those by Siess et al. (2000). The use of different PMS evolutionary models can introduce a systematic shift in the age estimation.

## 8.2 BRC regions

BRCs are considered to be a sort of remnant clouds originating from the dense parts (cores) in an inhomogeneous molecular cloud. So, if the original core was big enough, the resultant BRC could have undergone a series of RDI events (Kessel-Deynet & Burkert 2003), leaving

**Table 5.** Mean age inside/on the rim and outside rim

Region	Mean age (Myr)	
	Inside/On the rim (number of sources)	Outside rim (number of sources)
BRC NW	$0.92 \pm 0.56$ (12)	$1.29 \pm 0.54$ (19)
BRC 13	$1.61 \pm 1.41$ (10)	$2.44 \pm 1.37$ (24)
BRC 14	$1.01 \pm 0.73$ (18)	$2.32 \pm 1.22$ (58)

an elongated distribution of young stars. The distribution and evolutionary stages of such YSOs could be used to probe the star formation history in the HII regions. Using *Spitzer* observations Koenig et al. (2008) have identified clustered and distributed population of YSOs in W5 (see their figure 12). The clustered population shows a nice alignments of Class II sources towards the directions of BRCs from the ionization sources. In Paper II, we also examined the global distribution of YSOs, the radial distribution of  $A_V$  as well as the amount of NIR excess  $\Delta(H - K)$ , defined as the horizontal displacement from the middle reddening vector in the NIR-CC diagram (see Fig. 6), in the BRCs 13 and 14 regions. On the basis of these distributions, star formation was found to have propagated from the ionising source in the direction of the BRCs.

Fig. 15 shows the global distribution of clustered YSOs selected from the study of Koenig et al. (2008), in the whole W5 E region, which indicates an alignment of YSOs towards the direction of the BRCs. Fig. 16 shows the radial variation of  $\Delta(H - K)$  and  $A_V$ , of the YSOs located within the strip towards the direction of BRC NW region. The distribution reveals higher  $A_V$  values near the BRC NW region.

On the basis of the global distribution of YSOs in the region and the radial distribution of the amount of NIR excess  $\Delta(H - K)$  and  $A_V$  in the region (cf. Figs. 16, 17 and figures 6, 7 and 8 of Paper II) as well as the age distribution of YSOs, it seems that a series of RDI processes proceeded in the past from near the central O star towards the present locations of the BRCs.

### 8.2.1 Small scale sequential star formation ( $S^4F$ )

There has been qualitative evidence for the  $S^4F$  hypothesis such as an asymmetric distribution of probable TTSs (Ogura et al. 2002) and of the properties of NIR excess stars (Matsuyanagi et al. 2006). Papers I and II presented some quantitative evidence on the basis of  $BVI_C$  photometry. In the present study the sample of YSOs is significantly larger as compared to that used in Papers I and II. To further verify the  $S^4F$  hypothesis we follow

the approach as given in Papers I and II. We have divided the YSOs associated with BRCs into two groups: those lying inside/on the rim (i.e., stars embedded or projected onto the molecular cloud/lying on the rim) and outside the rim (i.e., stars lying outside the rim in the projected HII region) (see e.g., Figure A1 of Paper II for BRCs 13 and 14). Mean age has been calculated for these regions. Since the ionising source of the BRCs studied here has a maximum MS lifetime of 4-5 Myr, therefore the sources having age greater than 5 Myr can not be expected as the products of triggered star formation. They might have formed spontaneously in the original molecular cloud prior to the formation of the HII region. Some of them may be background stars; larger distances make them look older in the CM diagram. Therefore, while calculating the mean age we have not included those stars. The results are given in Table 5, which shows that in all the BRCs, the YSOs lying on/inside the rim are younger than those located outside it. The above results are exactly the same as those obtained in Papers I and II. Therefore, the present results further confirm the  $S^4F$  hypothesis. As in Papers I and II, we again find a large scatter in the stellar age in spite of a clear trend of the mean age. Possible reasons for the scatter, as discussed in earlier papers, include photometric errors, errors in extinction correction, light variation of young stars, drift of stars due to their proper motions, binarity of the stars, etc. Photometric errors and light variation as big as 0.5 mag would affect stellar ages by 0.25 dex, so they do not seem to be the major reason for the scatter. As for the extinction correction, it probably does not affect the results much, since in the  $V$ ,  $(V - I_c)$  CMD the reddening vector is nearly parallel to the isochrones. As discussed in Papers I and II, we speculate that the proper motions of the newly born stars may probably be the main cause of the scatter.

## 9 EVOLUTION OF DISKS OF T-TAURI STARS

$H\alpha$  emission and IR excess are important signatures of young PMS stars. These signatures in CTTSs indicate the existence of a well-developed circumstellar disk actively interacting with the central star. Strong  $H\alpha$  emission (equivalent width  $EW > 10 \text{ \AA}$ ) in CTTSs is attributed to the magnetospheric accretion of the innermost disk matter onto the central star (Hartmann et al. 1994; Edwards et al. 1994; Muzerolle et al 2001 and references therein). On the other hand the weak  $H\alpha$  emission ( $EW < 10 \text{ \AA}$ ) in weak-line T Tauri stars (WTTSs), which lack disks (or, at least inner disks), is believed to originate from their chromospheric activity (e.g., Walter et al. 1988; Martín 1998). In the 1990s, a large number of WTTSs were

found in and over wide areas around T-associations by X-ray surveys with ROSAT, which led to active studies on the nature of the so-called dispersed WTTs.

The “standard model” (Kenyon and Hartmann 1995) postulates that the CTTs evolve to the WTTs by losing their circumstellar disk (or, at least its inner part). The age distribution derived from the HR diagram of the Taurus region indicates that the WTTs are systematically older than the CTTs, but the statistical significance is low (Kenyon and Hartmann 1995; Hartmann 2001; Armitage et al. 2003). Bertout et al. (2007) concluded that the observed age and mass distribution of CTTs and WTTs in the Taurus-Auriga T association can be explained by assuming that a CTT evolves into a WTT. In Paper II we compared the age distribution of CTTs and WTTs associated with several BRCs and supported the conclusion of Bertout et al. (2007).

On the other hand, there have also been many observations which claimed that the CTT and the WTT are coeval and have indistinguishable age distribution (e.g., Walter et al. 1988; Lawson et al. 1996; Gras-Velázquez & Ray 2005). From the analyses of the HR diagram of the CTTs and WTTs in Chamaeleon I, Lawson et al. (1996) concluded that some stars may be born even almost diskless or lose the disk at very early stages (age  $< 1$  Myr).

In the present work we have derived the age of 79, 26, 29, 59 Class II and 27, 5, 5, 17 Class III sources in the cluster, BRC NW, BRC 13, BRC 14 regions, respectively. Assuming that all the identified Class II and Class III stars are CTTs and WTTs respectively, we can study the possible evolution of the TTs. The advantage of our sample in addressing this issue is that the stars are spatially, i.e., three-dimensionally, very close to each other, so there should be no problem of distance difference, contrary to extended T associations. Here we would like to caution the readers that although we have attempted to clean the Class III sample from sources not belonging to W5, however, to confirm the WTTs nature of these sources in the absence of spectral information such as measurement of the Lithium absorption line is difficult.

Since data for Class III sources in the BRC NW and BRC 13 regions are not statistically significant, in Fig. 17 we show the cumulative distribution of Class II and Class III sources in the cluster and BRC 14 region only. Fig. 17 indicates that both the Class III and Class II sources have rather similar distribution. A Kolmogorov-Smirnov (KS) test for the combined sample of the cluster and BRC 14 region confirms the statement that the cumulative distributions of Class II sources (CTTs) and Class III sources (WTTs) are different only

at a confidence level of 50%. Hence, we can conclude that both the samples have rather similar distribution with practically indistinguishable age distribution. This result is in contradiction with that of Bertout et al. (2007) for the Taurus-Auriga T-association and that of Paper II, that WTTSs are older than CTTSs and CTTSs evolve into WTTSs; and it is in agreement with those which claim that the CTTSs and WTTSs are coeval and have indistinguishable properties. Here we have to keep in mind that the classification of CTTS and WTTS in the present work is based on the *Spitzer* MIR observations whereas in Paper II and in Bertout et al. (2007), the classification was based on the EWs of  $H\alpha$  emission stars.  $H\alpha$  surveys may fail to detect Class III sources which have smaller EWs whereas, those sources can be identified using the MIR observations. Here it is worthwhile to point out that the Class III sources by Koenig et al. (2008) were identified on the basis of all four *Spitzer* IRAC bands (3.6, 4.5, 5.8 and 8.0  $\mu\text{m}$ ). The detection of Class III sources would be suppressed because of less sensitivity at 5.8 and 8.0  $\mu\text{m}$  bands and also because of the very bright, variable background at these wavelengths in W5. Koenig et al. (2008) have stated that their photospheric sample is only 90% complete to 2  $M_{\odot}$  in general in W5, and to 8  $M_{\odot}$  on regions of bright background emission (e.g., the BRCs studied in this paper). This fact is evident in  $V/(V - I)$  CMD (Fig. 7) by comparing the number of Class II sources to the number of Class IIIs fainter than 20th magnitude in  $V$  band.

## 10 CONCLUSIONS

In this paper we have made  $VI_c$  photometric studies of the newly identified central cluster of W5 E. NIR data from 2MASS and MIR data from IRAC/MIPS of the *Spitzer* telescope have also been added to consider the properties of the cluster. Also, by incorporating *Spitzer* data we have re-analysed the properties (age and spatial distribution, etc.) of the YSOs in W5 E with special emphasis on the three BRC regions. We obtained the following as the main conclusion of the present work.

The central cluster has a distance of  $\sim 2.1$  kpc, a radius of  $6'$  and a mean age of  $\sim 1.3$  Myr. The reddening law is normal. The star formation in the cluster region is found to be non-coeval, with an age spread of  $\sim 5$  Myr. The slope of the IMF within the cluster region in the mass range  $0.4 \leq M/M_{\odot} \leq 30$  is found to be  $\Gamma = -1.29 \pm 0.03$ , which is comparable to the Salpeter value. In the mass range of  $0.2 \leq M/M_{\odot} \leq 0.8$ ; the CMFs of the YSOs associated with the three BRCs show a break in the slope at  $\sim 0.8 M_{\odot}$ . The CMFs indicate

that the cluster region and BRC NW have relatively more low mass YSOs in the mass range  $0.2 \leq M/M_{\odot} \leq 0.8$ .

The distribution of the YSOs in the W5 E region indicates that they are globally aligned from the ionising source towards the BRCs. A comparison of the average age of the YSOs lying on/inside and outside the bright rim indicates a quantitative age gradient in the sense that the YSOs located on/inside the rim are younger than those located outside the rim. The results are similar to those reported in Paper I and Paper II. These results confirm the  $S^4F$  hypothesis. The globally aligned distribution of the YSOs, indicate that a series of RDI events took place in the past from near the central ionising source to the periphery of the HII region.

In the present study it is found that the age distributions of the Class II and Class III sources are the same. This result is in accordance with the results which claimed that the CTTS and the WTTS are coeval and have indistinguishable age distribution (e.g., Walter et al. 1988; Lawson et al. 1996; Gras-Velzquez & Ray 2005).

## 11 ACKNOWLEDGMENTS

The authors are grateful to the anonymous referee for useful comments that improved the contents of the paper. We are thankful to the Kiso Observatory, IAO and ARIES for allotting the observing time. We also thank the staff of Kiso Observatory (Japan), IAO, Hanle and its remote control station CREST, Hosakote for their assistance during observations. This publication makes use of data from the Two Micron All Sky Survey, which is a joint project of the University of Massachusetts and the Infrared Processing and Analysis Center/California Institute of Technology, funded by the National Aeronautics and Space Administration and the National Science Foundation. NC is thankful for the financial support for this study through the fellowships granted by the DST and CSIR, India.

## REFERENCES

- Armitage P.J., Clarke C.J., Palla F. 2003, MNRAS, 342, 1139  
Becker W., Fenkart R. 1971, A&AS, 4, 241  
Bertoldi F. 1989, ApJ, 346, 735  
Bessell M.S., Brett J.M. 1988, PASP, 100, 1134  
Bertout C., Siess L., Cabrit S. 2007, A&A, 473, L21

- Chauhan Neelam, Pandey A.K., Ogura K., Ojha D.K., et al. 2009, MNRAS, 396, 694 (Paper II)
- Chini R., Wargau W. F., 1990, A&A, 227, 5
- Chini R., Krüegel E. 1983, A&A, 117, 289
- Cohen J.G., Frogel J.A., Persson S.E., Ellias J.H. 1981, ApJ, 249, 481
- Conti P.S., Leep E. M. 1974, ApJ, 193, 113
- Cutri R.M., Skrutskie, M. F., van Dyk, S., et al., 2003, The IRSA 2MASS All Sky Point Source Catalog, NASA/IPAC Infrared Science Archive, <http://irsa.ipac.caltech.edu/applications/Gator/>
- Edwards S., Hartigan P., Ghandour L., & Andrulis C. 1994, AJ, 108, 1056
- Georgelin Y.M., Georgelin Y.P. 1976, A&A, 49, 57
- Girardi L., Bertelli G., Bressan A., Chiosi C., Groenewegen M.A.T., et al. 2002, A&A, 391,195
- Gras-Velázquez A., Ray T. P. 2005, A&A, 443, 541
- Hartmann L., Hewett R., Calvet N. 1994, ApJ, 426, 669
- Hartmann L. 2001, AJ, 121, 1030
- He Lida, Whittet D. C. B., Kilkenny D., Spencer Jones J. H., 1995, ApJS, 101, 335
- Hillenbrand L.A., Strom S.E., Vrba F.J., Keene J. 1992, ApJ, 397, 613
- Hillenbrand L.A. 2005, A Decade of Discovery: Planets Around Other Stars” STScI Symposium Series 19, ed. M. Livio, eprint arXiv:astro-ph/0511083
- Hillenbrand L.A., Bauermeister A. & White R.J. 2008, in ASP Conf. Ser. 384, 14th Cambridge Workshop on Cool Stars, Stellar Systems, and the Sun, ed. G. van Belle (San Francisco, CA: ASP), 200
- Hillwig Todd C., Gies D.R., Bagnuolo W. G. Jr., Huang W., McSwain M. V., Wingert D.W. 2006, ApJ, 639, 1069
- Johnson H.L., Morgan W.W. 1953, ApJ, 117, 313
- Jose J., Pandey A.K., Ojha D.K., Ogura K., Chen W.P., Bhatt B.C., Ghosh S.K., Mito H., Maheswar G., Sharma S. 2008, MNRAS, 384, 1675
- Karr J.L., Martin P.G. 2003, ApJ 595, 900
- Kazarovets E.V., Durlevich O.V., Samus N.N. 1998, New Catalogue of Suspected Variable Stars, II/219, CDS, Strasbourg (NCSVS)
- Kenyon S., Hartmann L. 1995, ApJS, 101,117
- Kessel-Deynet O., Burkert A. 2003, MNRAS, 338, 545

- King I., 1962, AJ, 67, 471
- Koenig X.P., Allen L.E., Gutermuth R. A., Hora J.L., Brunt C.M., Muzerolle J. 2008, ApJ, 688, 1142
- Kroupa P. 2001, MNRAS, 322, 231
- Kroupa P. 2002, Science, 295, 82
- Landolt A.U. 1992, AJ, 104, 340
- Lawson W.A., Fiegelson E.D., Huenemoerder D.P. 1996, MNRAS, 280, 1071
- Lefloch B., Lazareff B. 1995, A&A, 301, 522
- Meyer M., Calvet N., Hillenbrand L.A. 1997, AJ, 114, 288
- Miao J., White G.J., Nelson R., Thompson M., Morgan L. 2006, MNRAS, 369, 143
- Martín E.L. 1998, AJ, 115, 351
- Martins F., Plez B. 2006, A&A, 457, 637
- Matsuyanagi I., Itoh Y., Sugitani K., Oasa Y., Mukai T., Tamura M. 2006, PASJ, 58, L29
- Morgan L.K., Thompson M.A., Urquhart J.S., White G.J. 2008, A&A, 477, 557
- Muzerolle J., Calvet N., Hartmann L. 2001, ApJ, 550, 994
- Nakano M., Sugitani K., Niwa T., Itoh Y., Watanabe M. 2008, PASJ, 60, 739
- Neckel T., Chini R. 1981, A&AS, 45, 451
- Niwa T., Tachihara K., Itoh Y., Oasa Y., et al. 2009, A&A, 500, 1119
- Ogura K., Sugitani K., Pickles A. 2002, AJ, 123, 2597
- Ogura K., Chauhan N., Pandey A.K., Bhatt B.C., Ojha D.K., Itoh Y. 2007, PASJ, 59, 199  
(Paper I)
- Ojha D.K., Tamura M., Nakajima Y., et al. 2004a, ApJ, 608, 797
- Ojha D.K., Tamura M., Nakajima Y., et al. 2004b, ApJ, 616, 1042
- Palla F., Stahler S.W. 1999, ApJ, 525, 772
- Pandey A. K., Ogura K., Sekiguchi K., 2000, PASJ, 52, 847
- Pandey A.K., Nilakshi, Ogura K., Sagar R., Tarusawa K. 2001, A&A, 374, 504
- Pandey A.K., Upadhyay K., Nakada Y., Ogura K., 2003, A&A, 397, 191
- Pandey A.K., Sharma S., Ogura K. 2006, MNRAS, 373, 255
- Pandey A.K., Sharma S., Ogura K., Ojha D.K., Chen W.P., Bhatt B.C., Ghosh S.K. 2008, MNRAS, 383, 1241
- Pandey et al. 2010, in preparation
- Robitaille T.P., Whitney B.A., Indebetouw R., Wood K., Denzmore P. 2006, ApJS, 167, 256
- Salpeter E.E. 1955, ApJ, 121, 161

- Samal M.R., Pandey A.K., Ojha D.K., Ghosh S.K., Kulkarni V.K., Bhatt B.C. 2007, ApJ, 671, 555
- Tamura M., Baba D., Sato S., Tsujimoto M. 2007, ApJ, 667, 963
- Schmidt-Kaler Th. 1982, Landolt-Bornstein, Vol. 2b, ed. K. Schaifers, H. H. Voigt, H. Landolt (Berlin: Springer), 19
- Siess L., Dufour E., Forestini M. 2000, A&A, 358, 593
- Stetson P.B. 1987, PASP, 99, 191
- Stetson P.B. 1992, ASPC, 25, 297
- Sugitani K., Fukui Y., Ogura K. 1991, ApJS, 77, 59
- Sugitani K., Tamura M., Ogura K. 1995, ApJ, 455, L39
- Tapia M., Costero R., Echevarria J., Roth M., 1991, MNRAS, 253, 649
- Turner N.H., ten Brummelaar T.A., Roberts L.C., Mason, B.D., Hartkopf W.I., Gies D.R. 2008, AJ, 136, 554
- Walborn N.R. 1973, AJ, 78, 1067
- Walter F.M., Brown A. Matthieu R.D., Meyer P.C., Vrba F.J. 1988, AJ, 96, 297
- Wegner W. 1993, AcA, 43, 209
- Winkler H. 1997, MNRAS, 287, 481

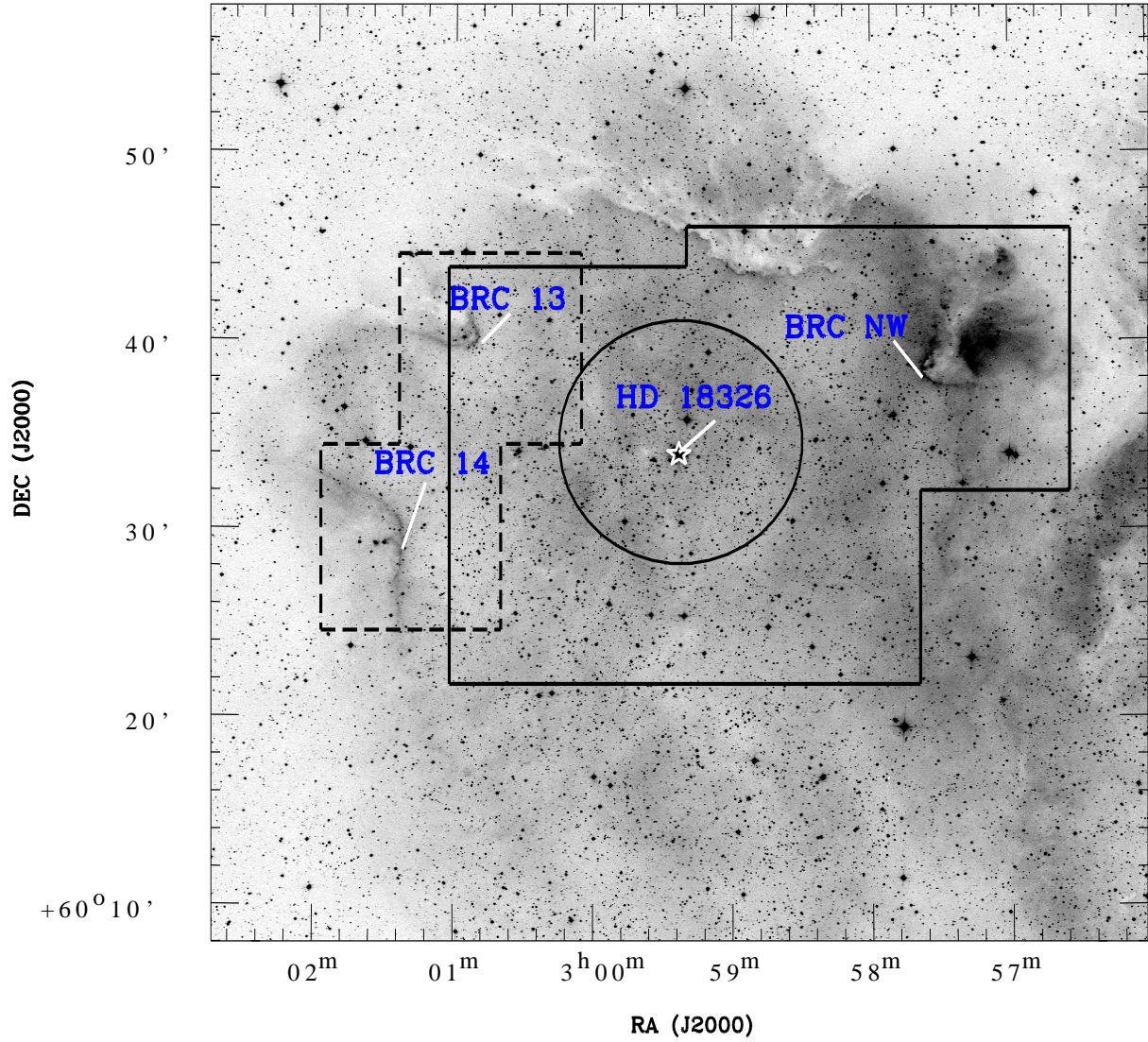


**Figure 1.** The  $50 \times 50$  arcmin<sup>2</sup> DSS2-R band image of the W5 E region. The area marked with thick lines is the region for which deep images are taken in V and  $I_c$  bands. The dashed lines represent the boundaries of the region for which we have used data from our earlier work (Paper II). The circle represents the boundary of the cluster. The abscissa and the ordinates are RA and DEC for the J2000 epoch.

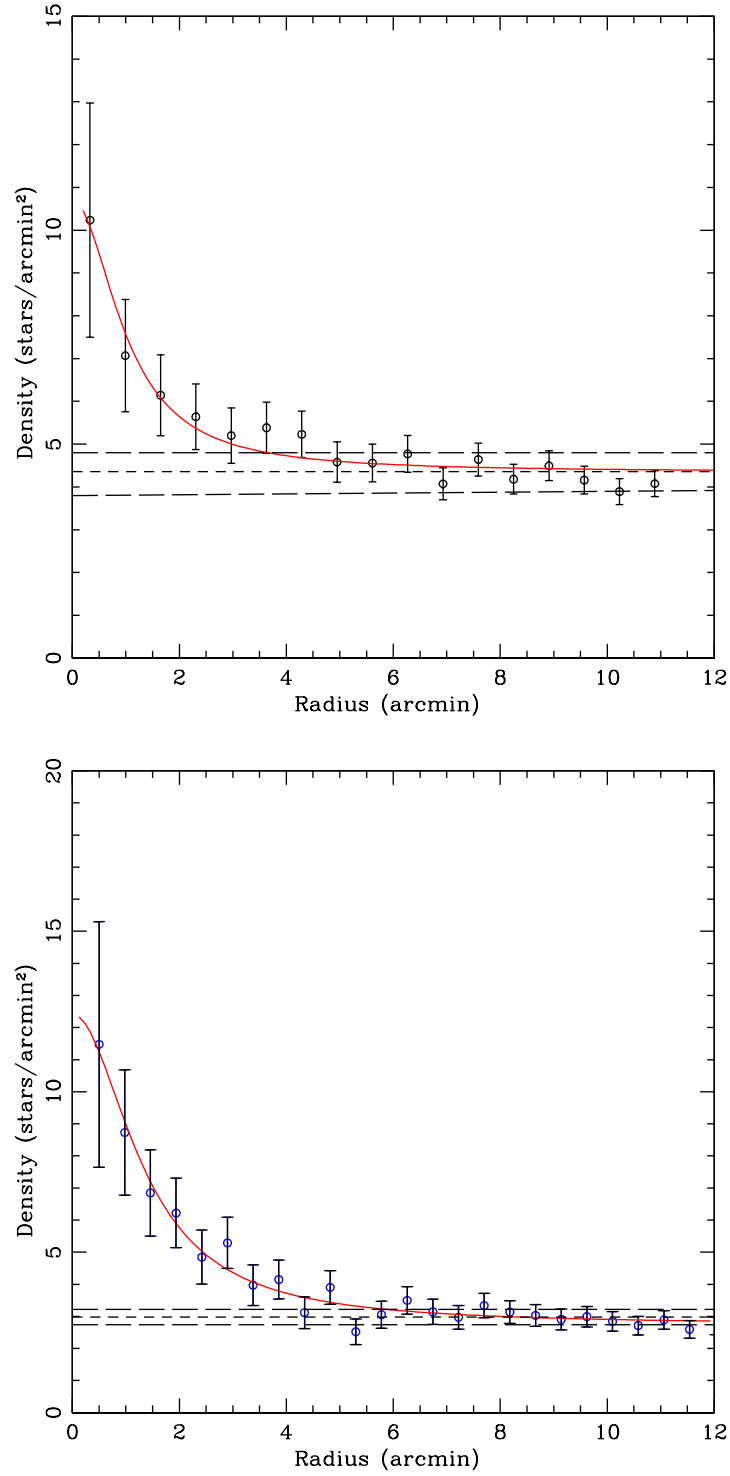


**Figure 2.** Radial density profiles for the cluster using the optical (upper panel) and 2MASS (lower panel) data. Thick dashed line represents the mean density level of the field stars and thin dashed lines are the error limits for the field star density. The continuous curve shows the least-squares fit of the King (1962) profile to the observed data points. The error bars represent  $\pm\sqrt{N}$  errors.

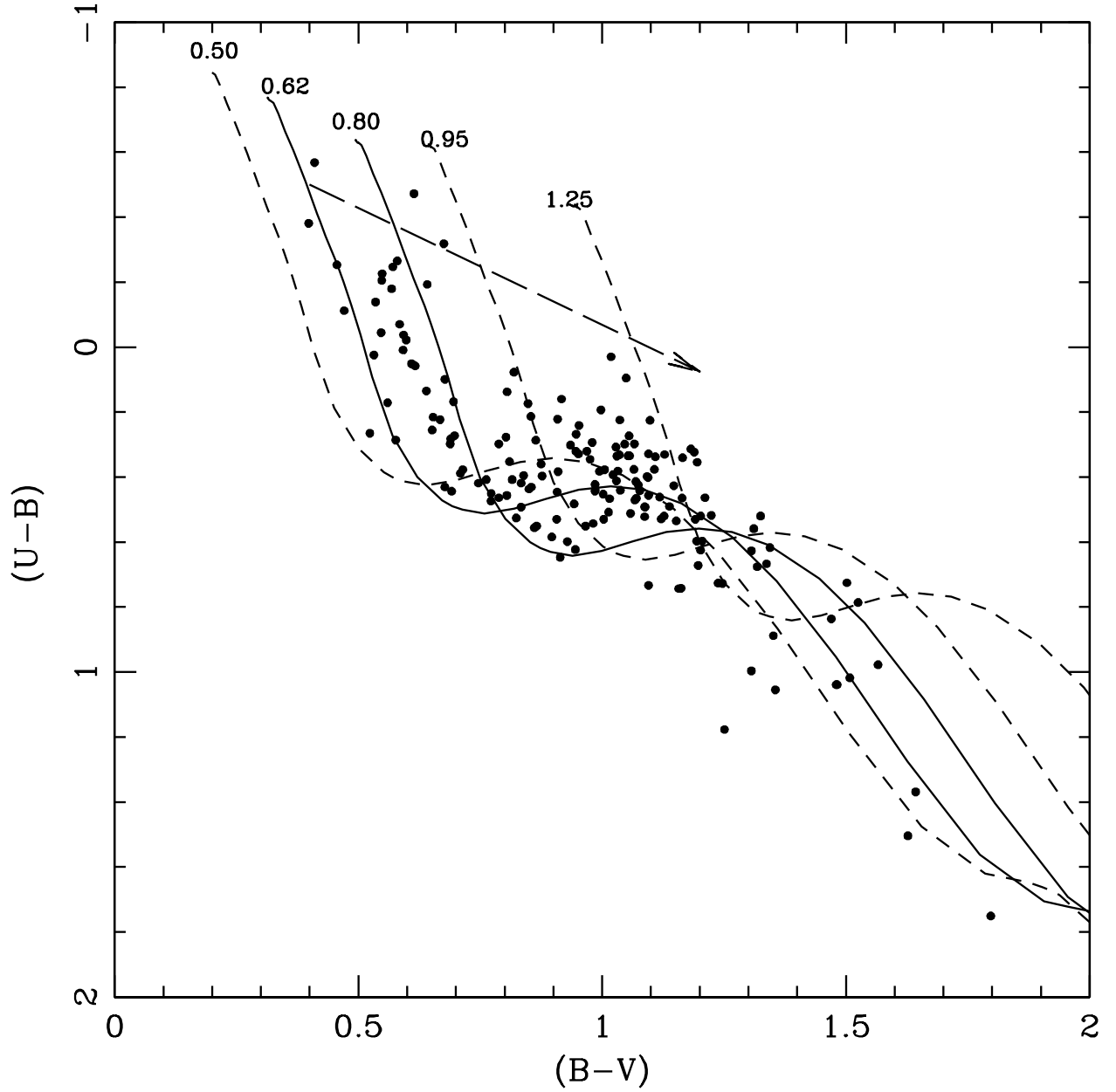


**Figure 3.**  $(U - B)/(B - V)$  CC diagram for the stars within the cluster radius ( $r_{cl} \leq 6'$ ). The continuous curves represent the ZAMS by Girardi et al. (2002) shifted along the reddening slope of 0.72 (shown as dashed arrow) for  $E(B - V) = 0.62$  mag and 0.80 mag, respectively. The dashed curves represent the ZAMS reddened by  $E(B - V) = 0.50$  mag, 0.95 mag and 1.25 mag, respectively to match the probable foreground and background populations (see the text for details).

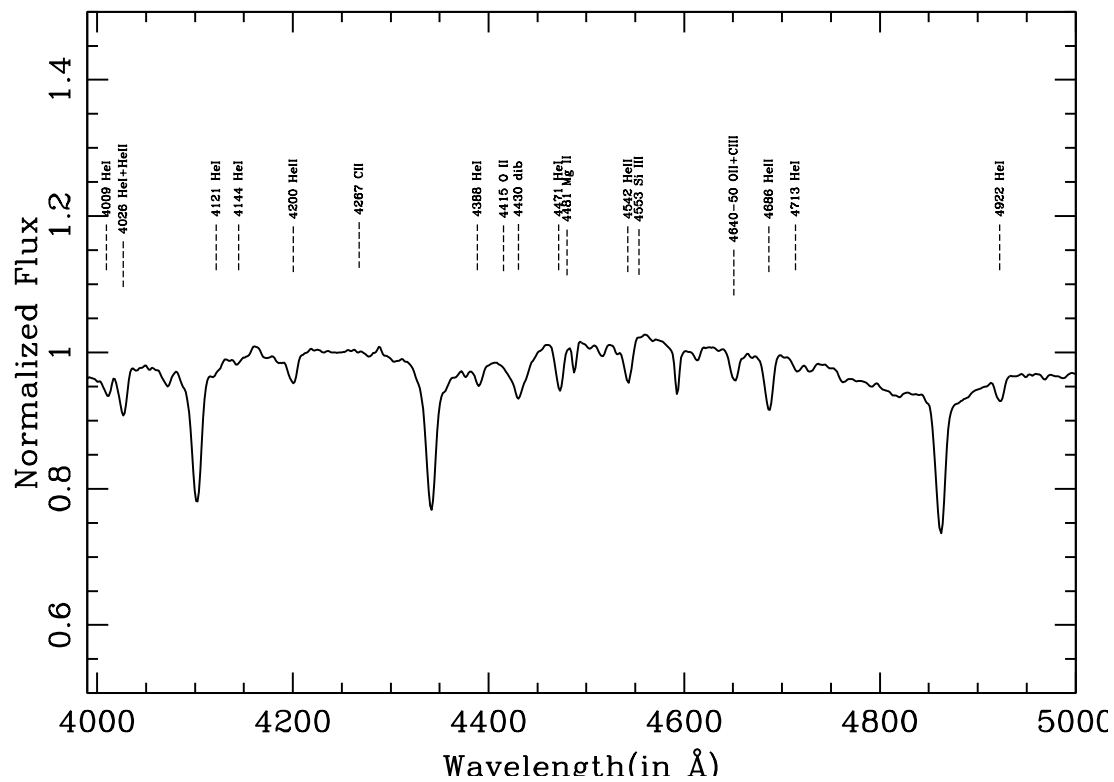


**Figure 4.** Flux calibrated normalised spectrum of HD 18326.

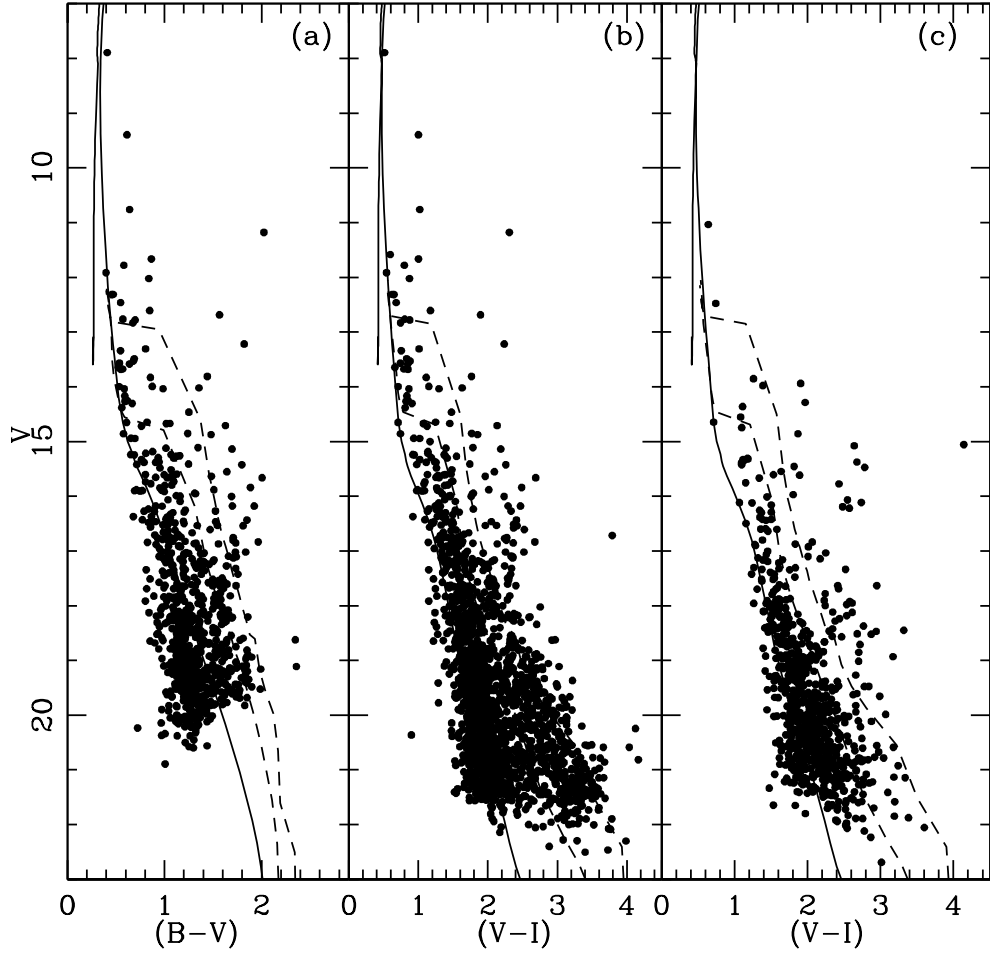


**Figure 5.** (a) and (b): The  $V/(B - V)$  and  $V/(V - I)$  CMDs for the stars within the cluster radius; (c):  $V/(V - I)$  CMD for stars in the field region having same area as in (a) and (b). The continuous line is the isochrone of 4 Myr from Girardi et al. (2002) and dashed lines are 1 Myr and 5 Myr PMS isochrones from Siess et al. (2000). The isochrones are corrected for the cluster distance of 2.1 kpc and reddening  $E(B - V) = 0.62$  mag.

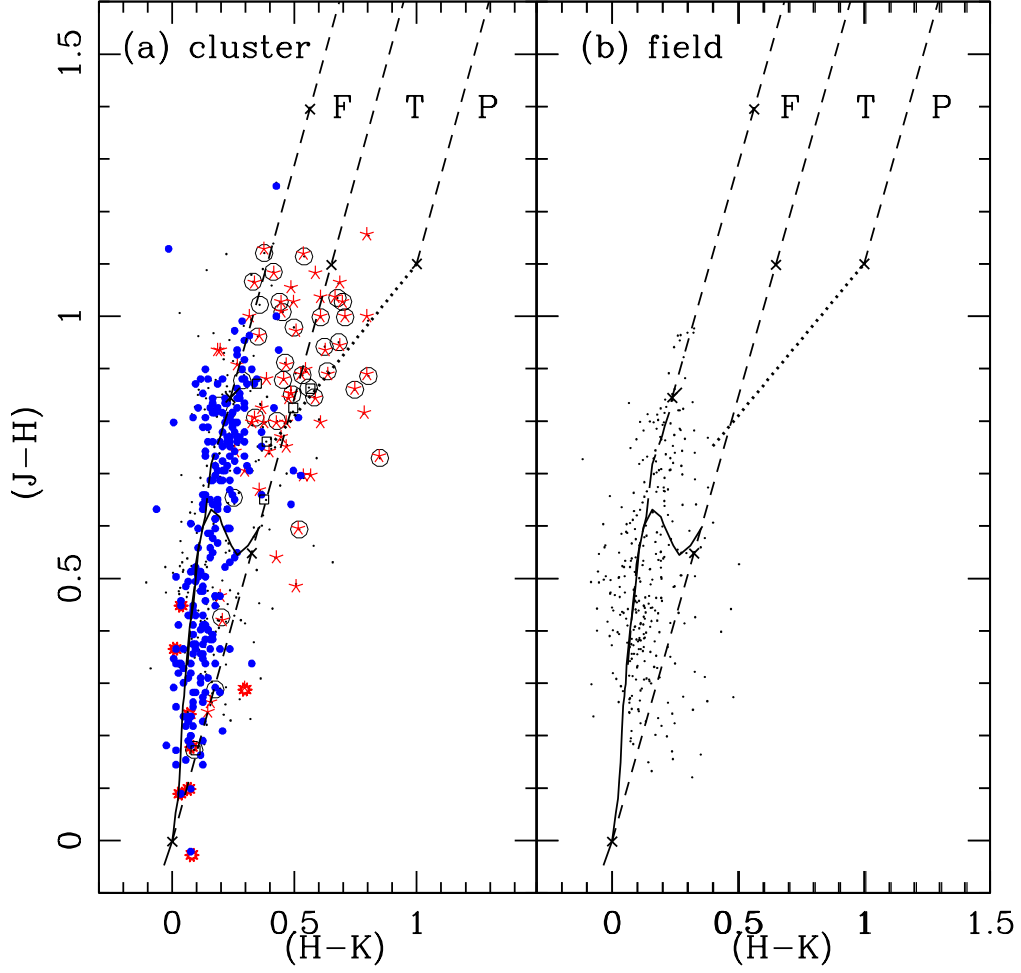


**Figure 6.** NIR  $(J-H)/(H-K)$  CC diagrams for the stars (a) within the cluster radius and (b) in the reference field. Small dots represent 2MASS sources and open circles represent  $H\alpha$  sources from Nakano et al. 2008. Class II, Class III and transition sources from the *Spitzer* photometry are shown by asterisks, filled circles and open squares, respectively. Dashed straight lines represent the reddening vectors (Cohen et al. 1981). The crosses on the dashed lines are separated by  $A_V = 5$  mag.

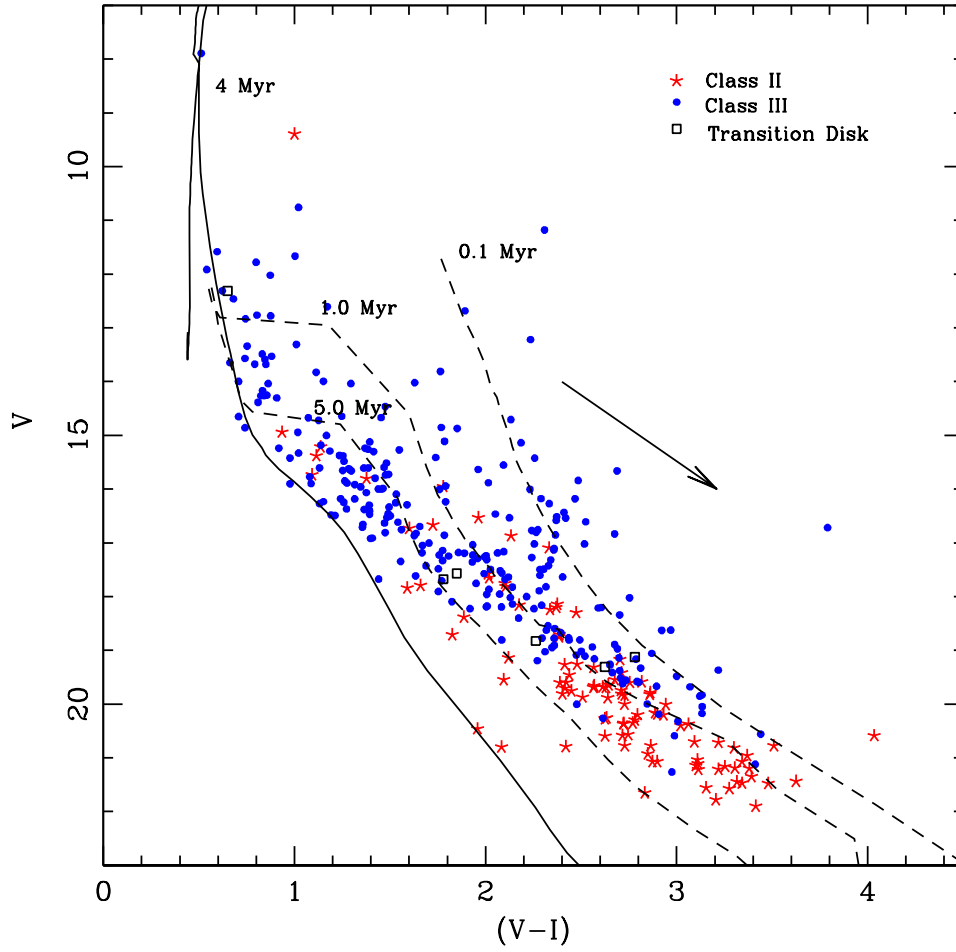


**Figure 7.**  $V/(V - I)$  CMD for the clustered YSOs identified by Koenig et al. (2008) in the cluster region. The continuous line is the isochrone of 4 Myr from Girardi et al. (2002) and dashed lines are the 0.1 Myr, 1 Myr and 5 Myr PMS isochrones from Siess et al. (2000). The isochrones are corrected for the cluster distance of 2.1 kpc and reddening  $E(B - V) = 0.62$  mag

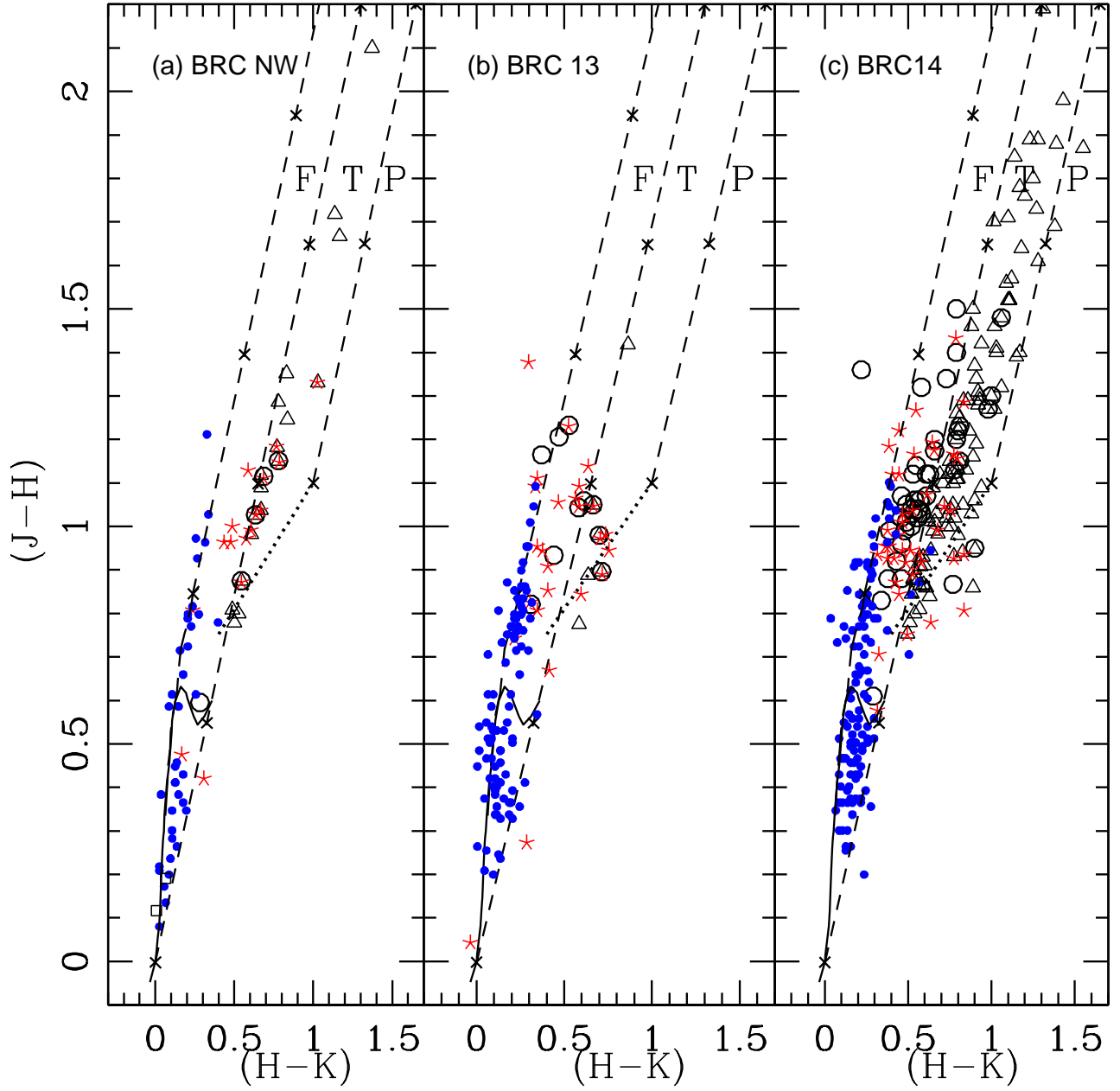


**Figure 8.** The  $(J - H)/(H - K)$  CC diagrams of the YSOs in the BRC NW, BRC 13 and BRC 14. Class I, Class II, Class III and transition sources from *Spitzer* photometry are shown by filled triangles, asterisks, filled circles and open squares, respectively. NIR excess sources from 2MASS and Matsuyanagi et al. (2006) (in case of BRC 14) are shown by open triangles and  $H\alpha$  sources from Ogura et al. (2002) are shown by open circles.

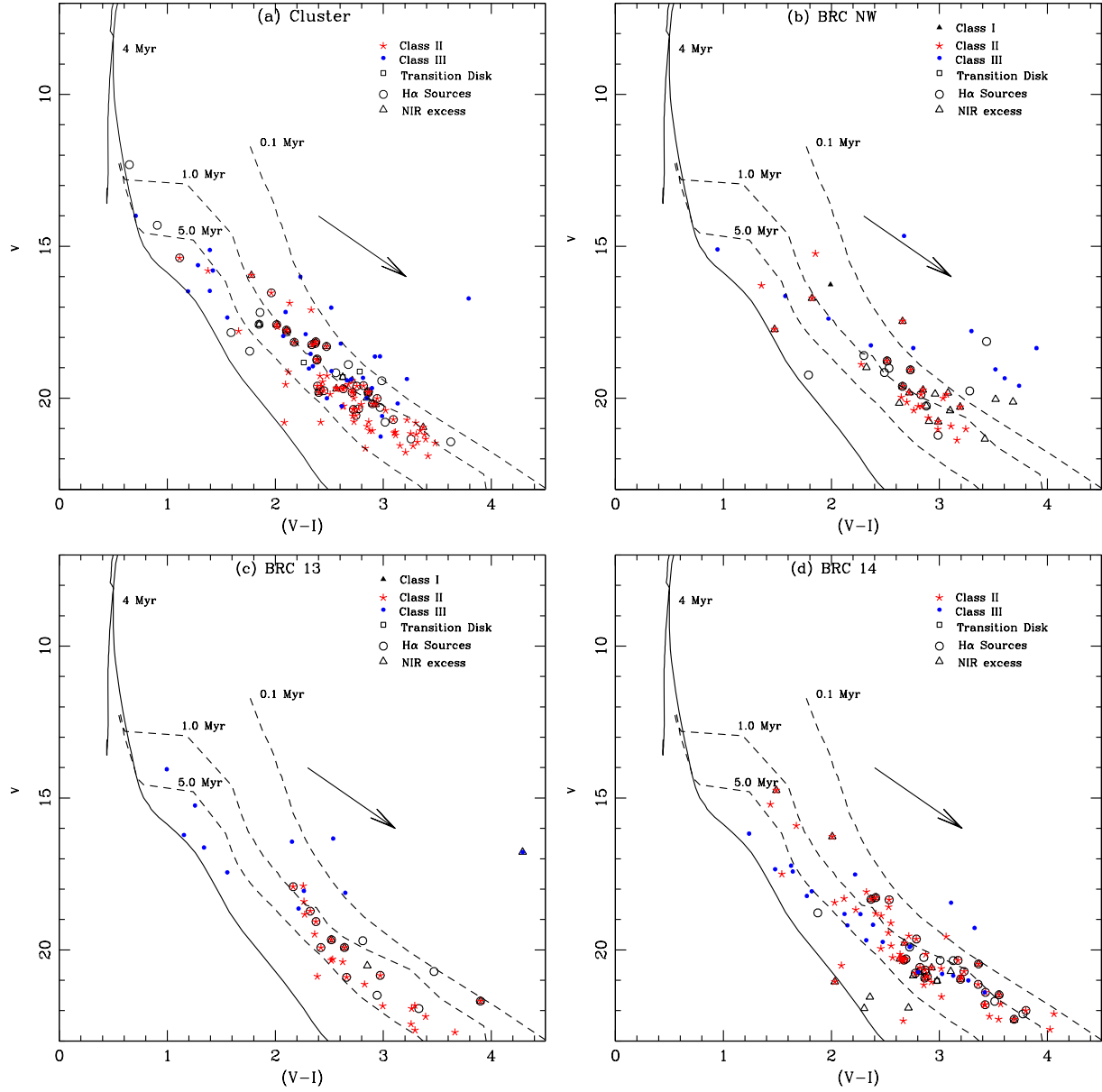


**Figure 9.**  $V/(V-I)$  colour-magnitude diagrams for the YSOs selected in the presented study (see the text) in the (a) cluster, (b) BRC NW, (c) BRC 13 and (d) BRC 14 regions. The continuous line is the isochrone of 4 Myr from Girardi et al. (2002) and dashed lines are 0.1, 1 and 5 Myr PMS isochrones from Siess et al. (2000). The isochrones are corrected for the distance and reddening of the respective regions. The arrow represents the reddening vector.

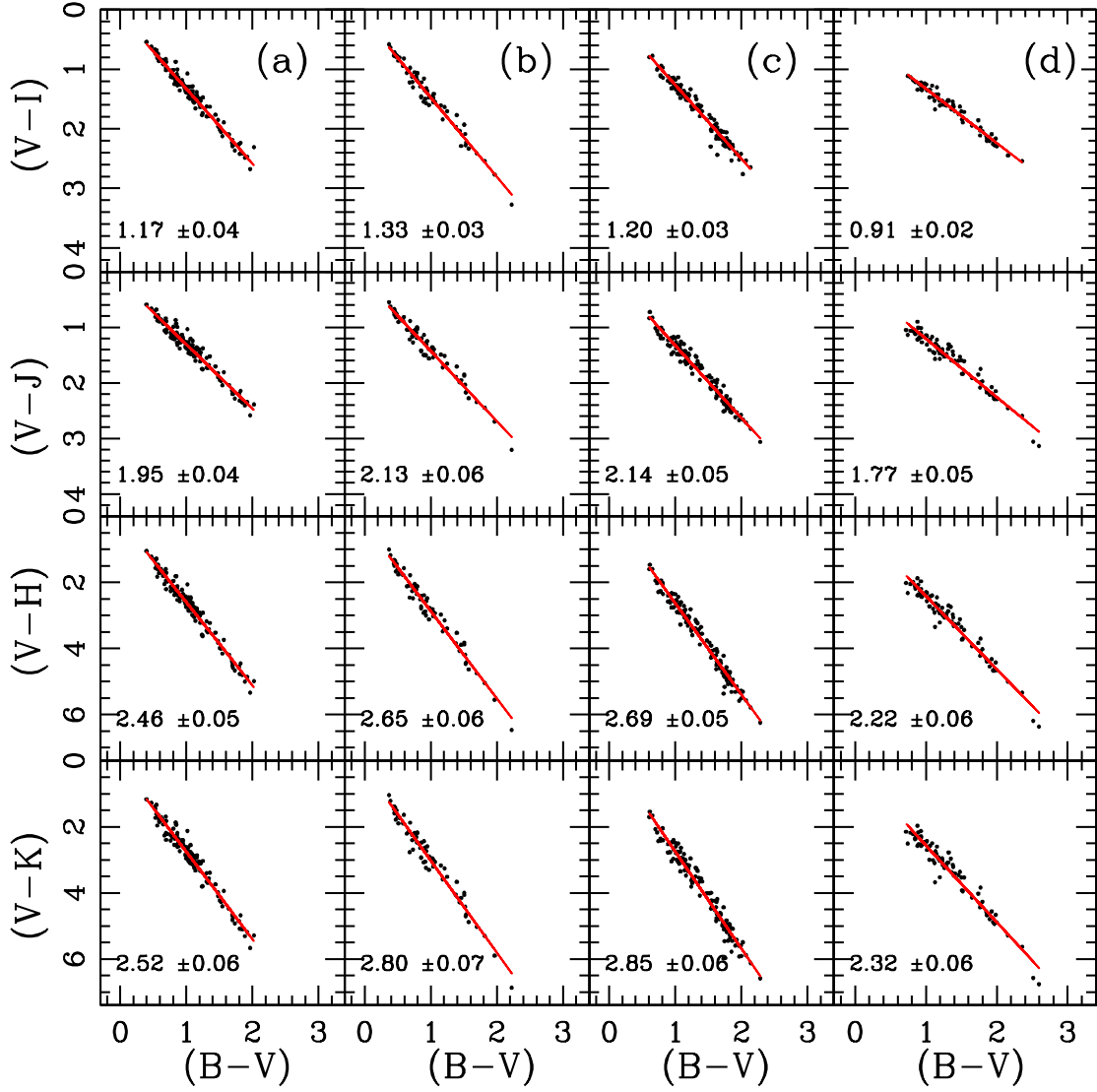


**Figure 10.** TCDs for the diskless (Class III) sources in the (a) cluster, (b) BRC NW, (c) BRC 13 and (d) BRC 14 regions.

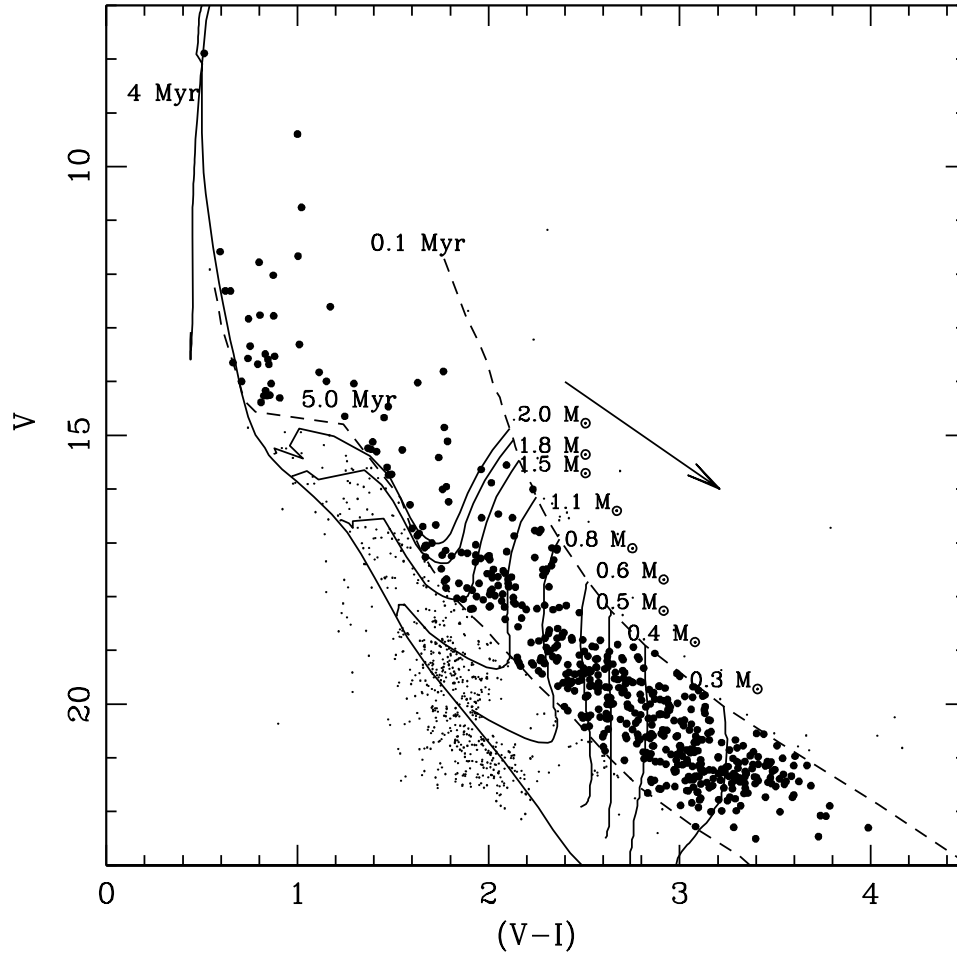


**Figure 11.** Statistically cleaned  $V/(V - I)$  CMD for stars lying within the cluster radius. The stars having PMS age  $\leq 5$  Myr are considered as representing the statistics of PMS stars in the region and are shown by filled circles. The isochrone for 4.0 Myr age by Girardi et al. (2002) and PMS isochrones of 0.1, 5.0 Myr along with evolutionary tracks for different masses by Siess et al. (2000) are also shown. All the isochrones are corrected for the cluster distance and reddening. The corresponding values of masses in solar mass are given at the right side of each track. Points shown by small dots are considered as non-members. The arrow represents the reddening vector.

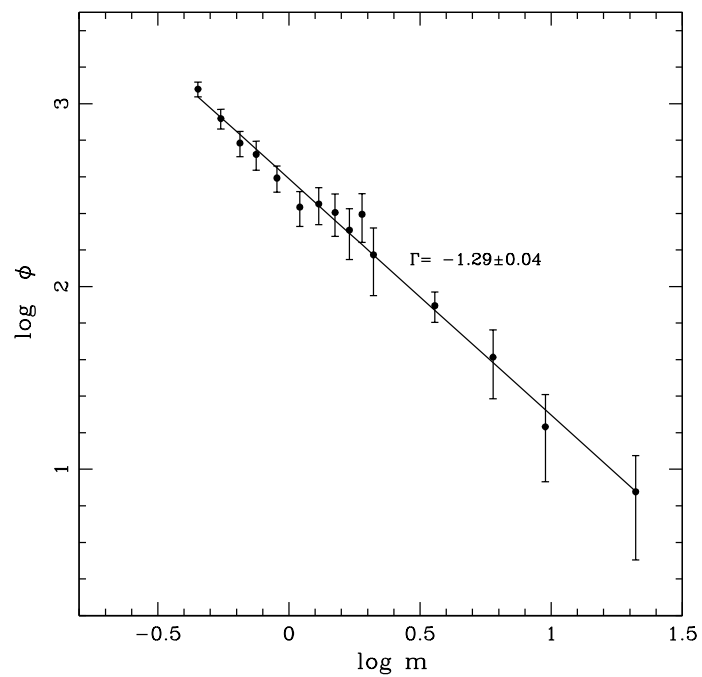


**Figure 12.** The MF in the cluster region derived using the optical data. The  $\phi$  represents  $N/d \log m$ . The error bars represent  $\pm\sqrt{N}$  errors. The continuous line shows least-squares fit to the mass ranges described in the text. The value of the slope obtained is mentioned in the figure.

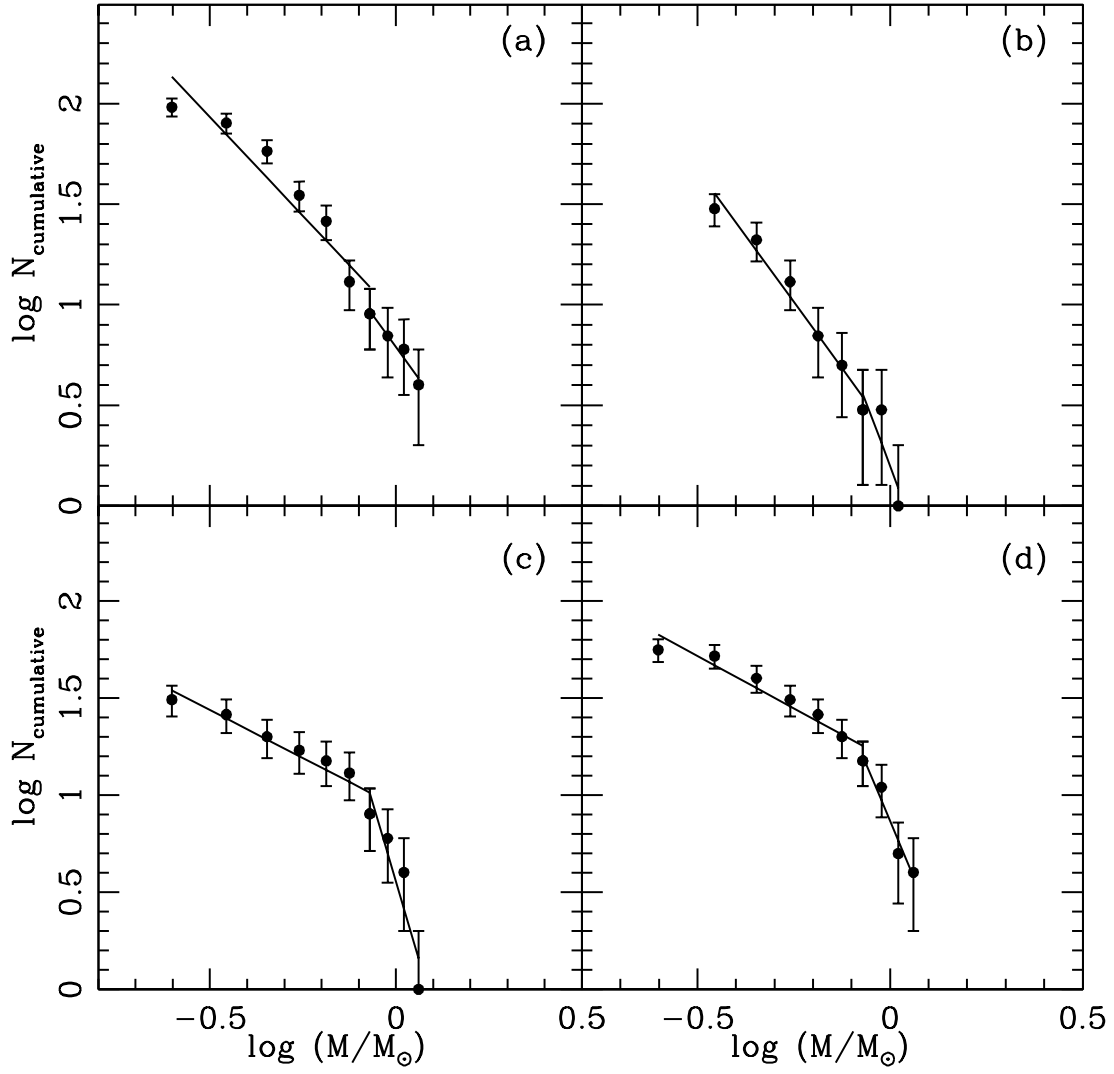


**Figure 13.** CMFs of YSOs in the (a) cluster, (b) BRC NW, (c) BRC 13 and (d) BRC 14 regions. Error bars represent  $\pm\sqrt{N}$  errors.

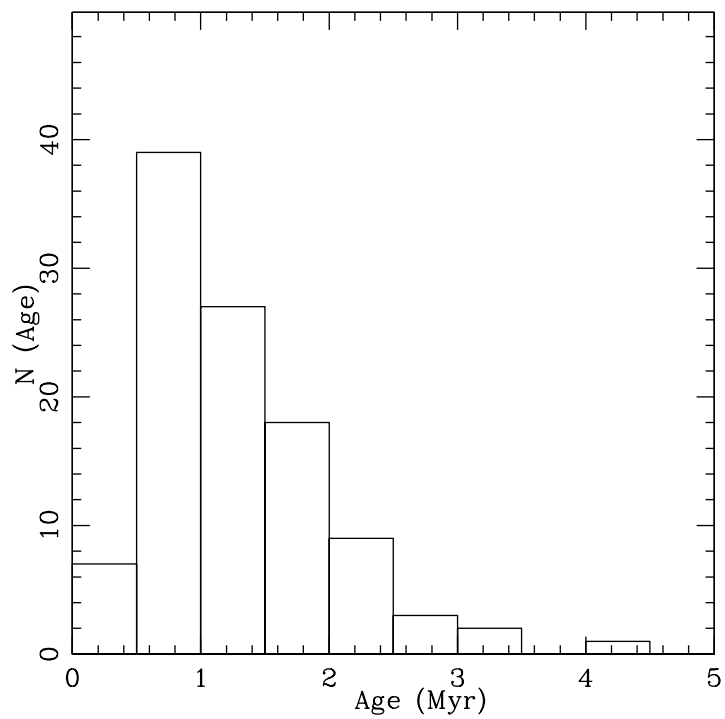


**Figure 14.** Histogram of the age distribution for the YSOs in the cluster region.

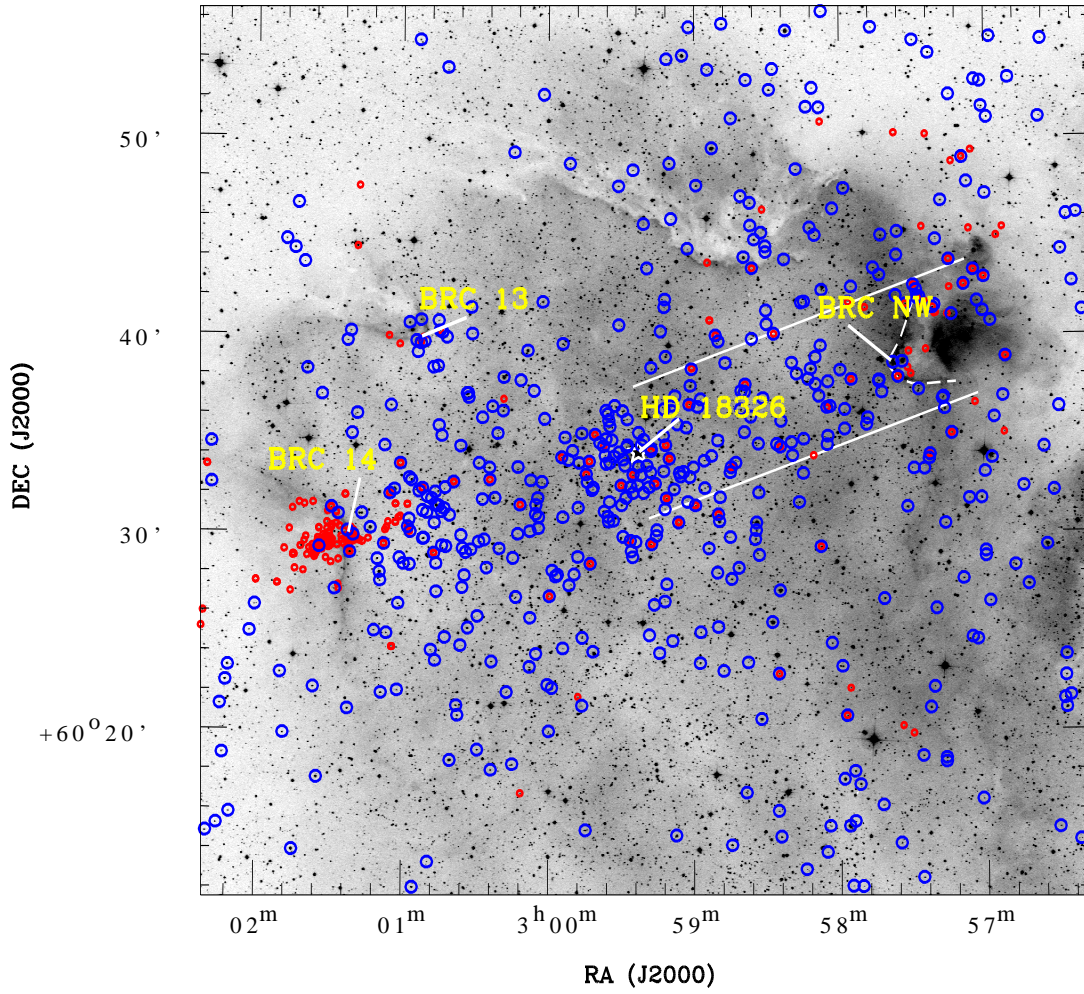


**Figure 15.** Global distribution of YSOs in the W5 E HII region. Small red circles show the location of NIR excess sources, whereas large blue circles (see the online version) show the YSOs identified using the *Spitzer* observations (see text).

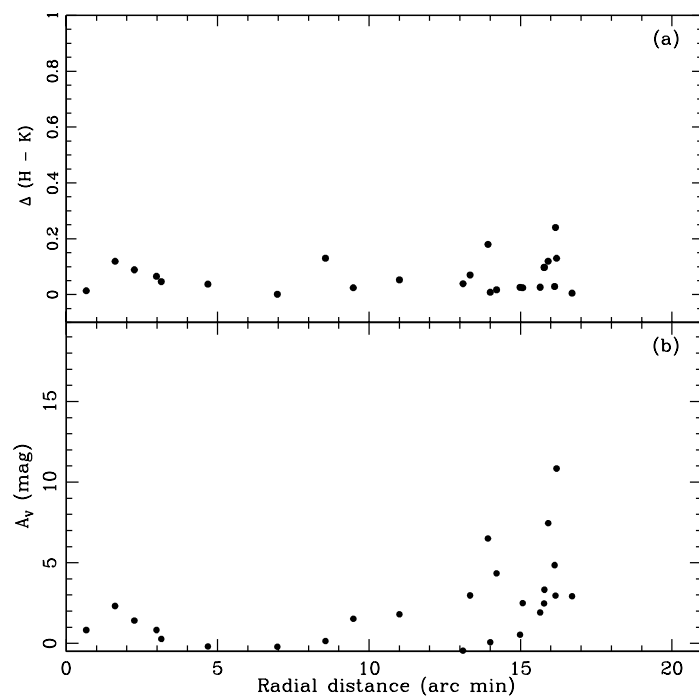


**Figure 16.** Variation of NIR excess  $\Delta(H-K)$  (upper panel) and  $A_V$  (lower panel) for the IR excess stars in the strip toward BRC NW as a function of distance from the ionising source (HD 18326) of the W5 E HII region.

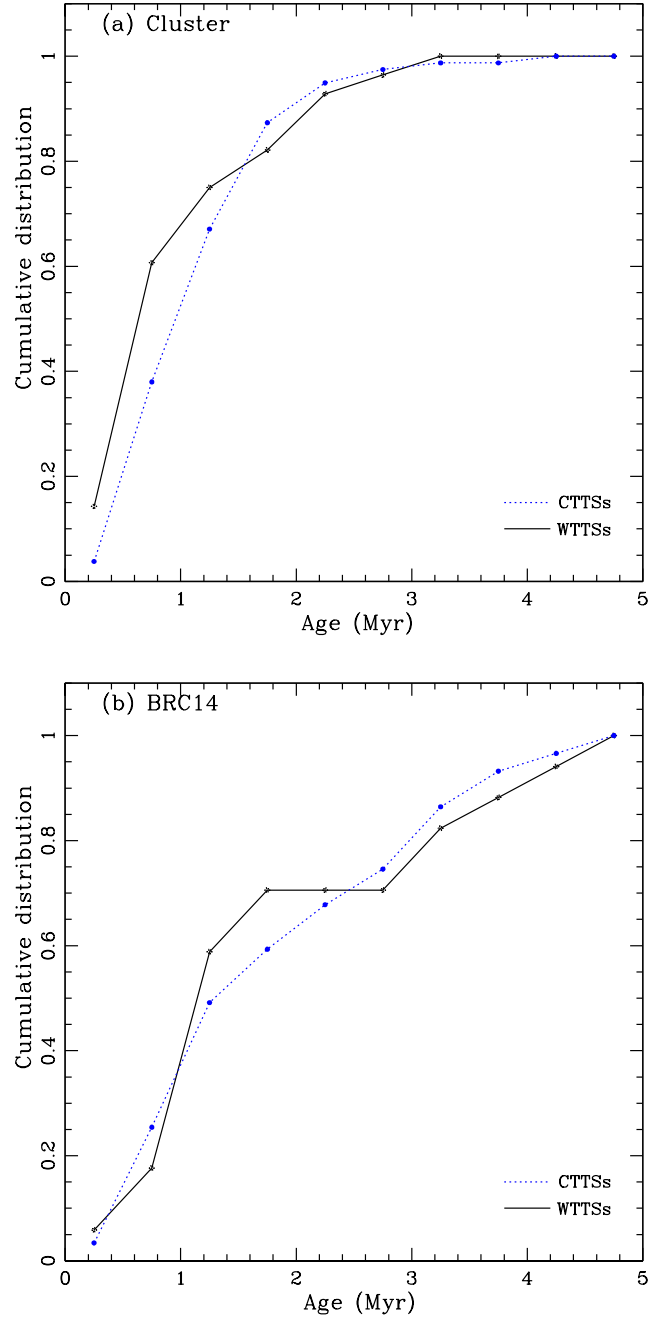


**Figure 17.** Cumulative age distribution of Class II (CTTSs) and Class III (WTTSs) sources in the (a) cluster and (b) BRC 14 region.

This paper has been typeset from a  $\text{\TeX}$ / $\text{\LaTeX}$  file prepared by the author.